QATAR UNIVERSITY

COLLEGE OF ENGINEERING

DESIGN, DEVELOPMENT, AND TESTING OF A TORQUE AND ANGLE MEASUREMENT SYSTEM FOR A TRACTION MACHINE

BY

MOHAMMAD FARHAN

A Thesis Submitted to

the College of Engineering

in Partial Fulfillment of the Requirements for the Degree of

Master of Science in Mechanical Engineering

June 2023

COMMITTEE PAGE

The members of the Committee approve the Thesis of
Mohammad Farhan defended on 14/05/2023

Dr. Mohammad Roshun Paurobally
Thesis Supervisor

Dr. Athol Thomson
Thesis Co-Supervisor

Dr. Sadok Sassi
Committee Member

Dr. Uvais Ahmed Qidwai
Committee Member

Dr. Wael alnahhal
Committee Member

Dr. Hassen Ouakad
Committee Member

Approved:

Khalid Kamal Naji, Dean, College of Engineering

ABSTRACT

FARHAN,MOHAMMAD, Masters :

June : 2023, Masters of Science in Mechanical Engineering

Title: Design, Development, and Testing of Torque and Angle Measurement System for a Traction Machine

Supervisor of Thesis: Dr. Mohammad Roshun Paurobally

This thesis presents the development of a traction measuring system designed to evaluate the interaction between shoes and playing surfaces to prevent lower extremity injuries. The interaction between shoes and playing surfaces has been identified as a key risk factor for lower extremity injuries. The traction system was designed and built with an advanced mechatronics interface which is going to be used as an add-on to an existing manually operated EXETER S2T2 traction machine utilized by Aspetar. The components of the traction machine such as the electronics interface, operating software, and connecting parts were developed in the workshop. The mechanical interactions such as rotational torque, and angular displacement, between the shoes and the natural grass as well as artificial grass of playing surfaces were measured. The values of torque were calculated at various applied loads within 90^{o} angles for inward and outward rotations, and it was plotted against the angular displacement, and speed of rotation. The peak torque obtained for the Nike Tiempo shoe has the highest traction of 32.44 Nm for outward rotation on natural grass (NG) and the lowest of 25.89 Nm for inward rotation on artificial grass (AG) which are considerably different for various loading and speed conditions. The result analysis shows the improved efficiency and ability of the mechatronic add-on over the existing manually operated traction

measuring machine. A numerical model was developed using the modified Bouc-Wen mode parameters for the calculation of torque with various conditions. The numerical results show that the rotational stiffness can be represented by sub-systems and each with their own properties. As the loading condition or speed changes, the model's degree of freedom also changes which leads to a reduction in sudden change in stiffness. The traction measuring system has the potential to contribute significantly to the understanding of lower extremity injury mechanics and to help design footwear and playing surfaces that minimize injury risk. The results of this study will be useful for sports medicine practitioners, footwear designers, and sports organizations looking to reduce the incidence of lower extremity injuries in athletes.

DEDICATION

This thesis is dedicated to my beloved father, Mohammad Idris, and my mother (Late), Mrs. Jaintun Nisha, as well as my family, for their unending efforts, support, and prayers, and for always being by my side. During my education, they appreciated, encouraged, and inspired me. Without them, I feel it would be impossible to attain this goal.

ACKNOWLEDGMENTS

I would like to express my sincere gratitude to my QU thesis Supervisor Dr. Mohammad Roshun Paurobally for his unwavering support, excellent guidance, and encouragement throughout my research. His expertise and constructive feedback were instrumental in shaping the direction and quality of this thesis. A special thanks to my Aspetar co-supervisor, Dr. Athol Thomson, for his support throughout my research work, specifically in providing the traction machine and demonstrating the manual working process of that machine. His discussions throughout this study have been very beneficial.

I am also grateful to my colleagues and friends who have provided me with support and encouragement throughout my academic journey. Their kindness and encouragement have been a source of motivation during the challenging moments.

I am indebted by gratitude to the world-class facilities and support of the Mechanical Workshop of Qatar University for providing me with a chance to carry out my entire research work and various materials to build my prototype.

TABLE OF CONTENTS

LIST OF TABLES

LIST OF FIGURES

CHAPTER 1: INTRODUCTION

1.1 Background

The most prevalent injuries in athletes' lower extremities are caused by inadequate or excessive traction between their shoes and the playing surfaces. The traction between the player's shoes and the playing surfaces is the most essential factor in the athlete's performance [1], [2]. For instance, an athlete’s shoe grip on the playing surface dictates how quickly the athlete can change maneuvers such as stopping, speeding up, and changing directions [3]–[6]. Non-contact lower extremity injuries account for 21-61% of lower extremity injuries in American football and soccer. These injuries are not the result of a direct load from another athlete or an object [7]–[11]. There are several types of playing surfaces that are employed in sports. These surfaces can be divided into two types: natural and artificial [12], [13]. The artificial surfaces are of the infill variety, with a base such as concrete or artificial grass fibers [14]–[16]. The common factors which affect the interactions between the shoes and the surface are the type of playing surface and the shoes used according to that surface. Shoes are categorized based on their playing surfaces, such as stud, edge, and fin types [17] as presented in Fig. 1. The stud-type shoes which mostly used in football are Conical, Bladed, Screw-in, and Hybrid Studs [18].

Figure 1. Various types of shoes used in football

Nowadays surfaces made of natural grass, artificial grass, or a combination of the two, which are known as hybrid reinforced grass systems are becoming widely attractive in a variety of sports, including football, soccer, and hockey [5], [19], as displayed in Fig. 2.

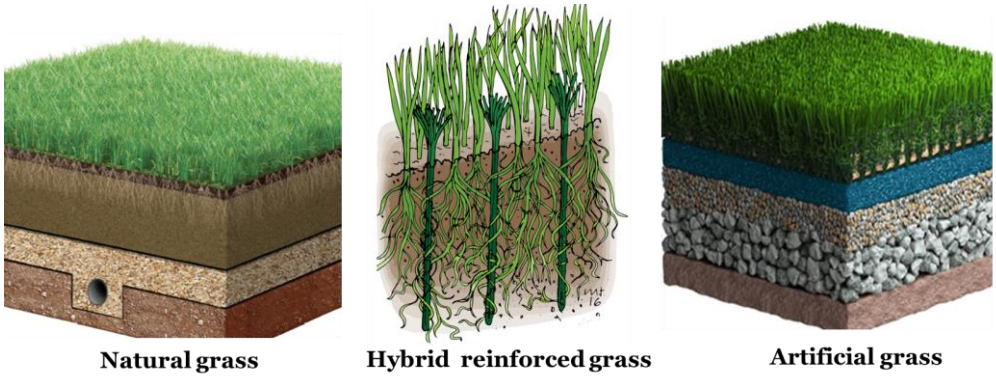

Figure 2. Different types of grass used for sports

Artificial grass fields were created to replicate the playing features of natural fields in an effort to promote participation in sports while lowering expenses [13], [20]. Every sport has fundamental characteristics designed to meet the requirements of the sport, which may be done by selecting the suitable surface specification as well as footwear

[21]–[23]. The design of the football shoe, as well as its compatibility with the playing surface, are essential for ensuring both good performance and injury prevention [24], [25]. Using the proper equipment, for instance, a traction machine [26], [27], the appropriate interaction between the shoes and the surface in different climate regions can be determined. Several traction machines, like the EXETER S2T2 [18], The BEAST (Biocore Elite Athlete Shoe-Surface Tester) [19], Boise State TurfBuster [28], Shoe traction and impact tester (STIT) [21], and The Pennfoot traction tester [29], are being utilized to analyze the mechanical interactions between the player's shoes and the playing surfaces as shown in Fig. 3(a),(b),(c). The BEAST is comprised of a foot shape attached to a shaft that can move vertically as well as horizontally along an interior support structure. The foot form was stiff for the testing presented here, and only the cleated part of the shoe was examined. The interior supporting frame can move vertically on a massive outer frame as indicated in Fig. 3(a) [7], [19]. The TurfBuster concept features an entirely automated testing system that controls translational and rotational motion as well as loading conditions with limited user input. It is made up of three major assemblies: the outside frame, the inner frame, and the dynamic motion assembly. The outer frame serves as a support framework for both the inner frame and the dynamic motion assembly, as well as the housing for the compressed-gas cylinders as displayed in Fig. 3(b) [28]. The Pennfoot is made up of a frame that holds a steel leg with a cast aluminum foot affixed to the bottom. Commercially available athletic footwear can be fitted to synthetic foot. All traction measures were obtained by placing the forefoot on the ground and the heel lifted off from the surface. Each of the measurements was taken with the shoe turned 45o. In between experiments, Pennfoot was relocated to the playing field as depicted in Fig. 3(c) [29]. The precision of these traction machines can offer a better understanding of the interaction between the shoes

and the surfaces, which can lead to a significant reduction in lower extremity injuries. In the field of sports, traction machines are used by specialists to determine the root cause of lower extremity injuries in players by assessing the necessary friction between the shoes and the playing surfaces [30]–[32]. Most traction machines are manufactured as a single unit which is bulky in size and usually manually operated with limited capabilities and required more manpower to operate it. Results may also not always be completely repeatable.

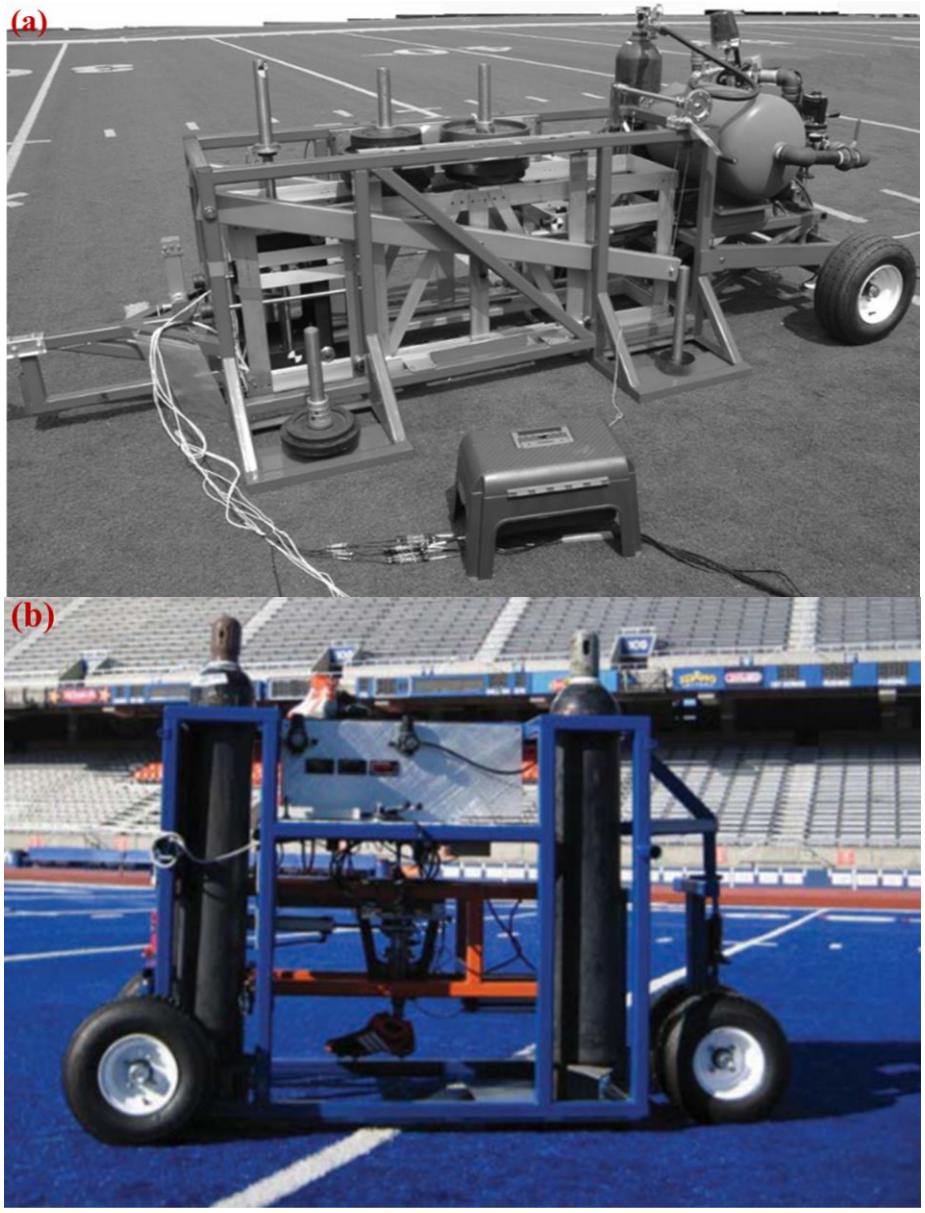

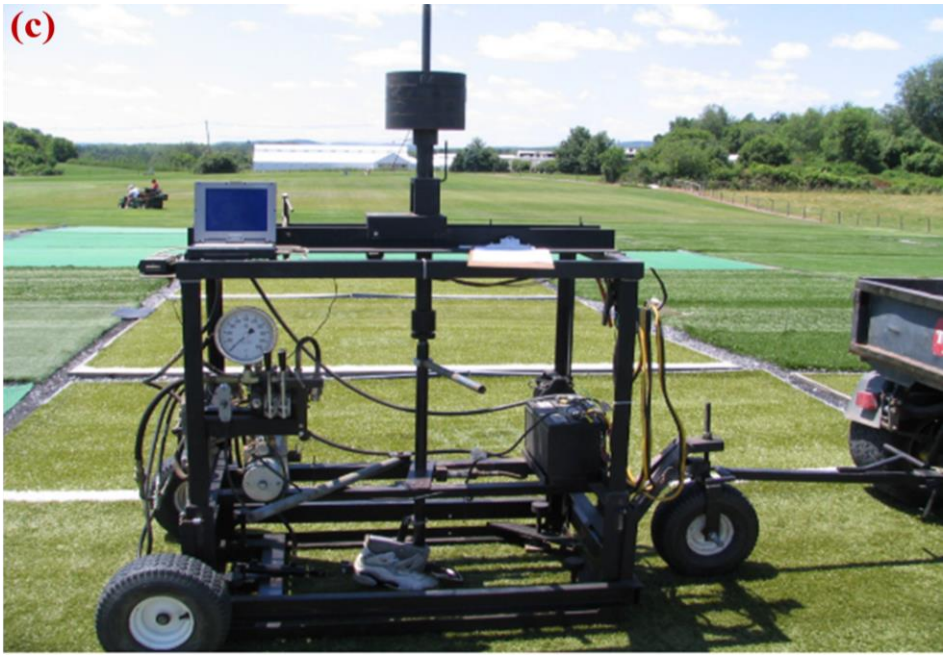

Figure 3. Different types of traction machines (a) BEAST (Biocore Elite Athlete Shoe-Surface Tester), (b) Boise State TurfBuster, (c) Pennfoot traction tester are currently used

To improve accuracy and yield better results while reducing physical labor during actual measurements, automation of manually operated machinery is required in a wide range of research domains [33]. Till now no research has provided continuous-time Torque and angle data. The current study addresses this gap and provides a new opportunity to study traction via the determination of rotational stiffness for various conditions.

This research presents the design, development, and testing of a mechatronic system add-on for the EXETER S2T2 traction machine [18], as seen in Fig 4.

Figure 4. EXETER S2T2 traction testing machine

This traction machine is manually operated and offers limited results when testing traction. It is also time-consuming and difficult to use since a large number of tests must be performed in order to acquire good results because only one value, the peak value, can be retrieved in one operation, which changes with each test. The angle of rotation cannot be determined with a torque wrench, raising concerns regarding torque and its relationship with angular rotation. In this project, an engineering design methodology is employed to design and build a mechatronic product add-on for the EXETER S2T2 traction machine. This system's functioning is automated by offering an interface so that test results can be easily accessible, hence broadening the scope of gathering data in a timely and effective manner. This includes using a dedicated torque and angle measurement sensor, a motor to provide rotation of the shoe, and an interface to obtain and display continuous-time results on screen as well as data capture and analysis.

1.2 Goals and Objectives

This project aims at delivering a novel add-on system of traction measuring along with the improvement in the testing method for the existing EXETER S2T2 traction machine to minimize the operating time and improve outcomes. The add-on system will be fabricated according to the physical parameters of the traction machine such as

dimensions and existing measurement system. The project will also aim to bring about a more concise and repeatable procedure for the evaluation of traction between shoes and playing surfaces.

The objectives of the project can be summarized as follows:

- To design and assemble the components to a frame that fits the product add-on using a Computer Aided Design package such as SolidWorks. The components include the motor, torque, and an angle sensor, which are connected between the motor, sensor, and dummy foot holding shaft.
- To design all the accessories such as mountings, fittings, frame, and wire housing as required for the operation of the system.
- To design the system and electronic interface comprising of a motor driver, sensor interface, and power supply. To create software that will record and display the results in real-time in a coordinated and visual manner. To collect pertinent data for subsequent processing.
- To test the entire automated traction system in the lab as well as in a real-world application and compare its precision with the existing manually operated system used by Aspetar.
- To recommend any additional capability of the system to enhance research output and improve knowledge.

CHAPTER 2: DESIGN AND DEVELOPMENT OF A MECHATRONIC ADD-ON

2.1 System's Components and Specifications

A system can be defined as a collection of components that work together to achieve a common goal. The components such as the system frame, housing box, and connecting shaft were designed and manufactured. The worm-geared drive DC motor and rotary torque sensor which are used in this system are described with their specifications. The Arduino and motor microcontroller are acquired according to the requirement of the system to achieve the best result possible.

2.1.1 Worm Geared Drive DC Motor

A worm-geared drive DC motor is a type of motor that utilizes a worm gear reduction mechanism to reduce the speed of the motor while increasing its torque output. The worm gear has meshed with a larger spur gear, which results in a gear reduction ratio of 50:1. This DC motor was chosen due to the project's required peak torque of ~100 Nm and a safety factor of 150 Nm capacity. The DC motor provides the rotational power to drive the worm gear, which in turn drives the spur gear. This type of motor is commonly used in applications that require slow movements, and high-torque operation, such as conveyors, material handling equipment, and robotics. Instead of manual rotation, a 600W 12V (063) NMRV worm-geared drive DC motor from Motion Dynamics [34], was employed to automate the traction testing as shown in Fig. 5.

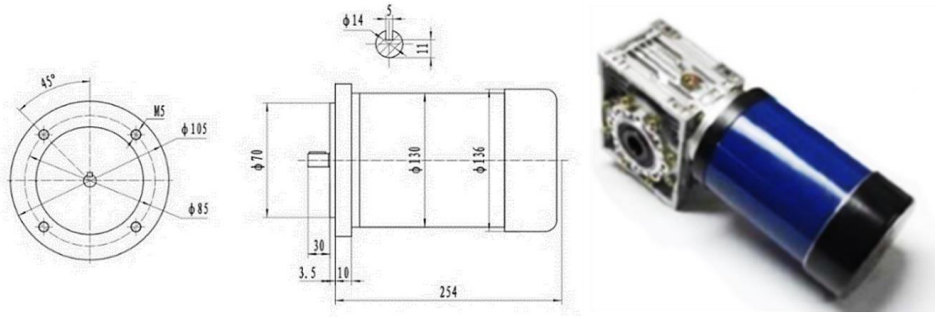

Figure 5. Worm-geared drive DC motor with dimensions from Motion Dynamics

Table 1. Specification Of worm geared drive DC motor

Parameters	Values
Weight	17.0 kg
Length	421 mm
Gear ratio	50:1
Voltage	12 V
Rated current	50 Amps
Power	600 W
Maximum speed	30 RPM
Maximum torque	150 Nm

2.1.2 FUTEK Rotary Torque Sensor

A rotary torque sensor is a type of sensor used to measure torque in rotary systems. It works by detecting the twisting force (torque) applied to a rotating shaft and converting it into an electrical signal. The signal can then be processed and analyzed by a data acquisition system to provide real-time measurements of torque. In this research, a FUTEK TRD305 rotary torque sensor was selected [35]. FUTEK rotary torque sensors are commonly used in a variety of applications, such as testing and validation of mechanical systems, motor control, and process control. They are known for their high accuracy, reliability, and robustness in harsh environments.

Figure 6. FUTEK rotary torque sensor

Table 2. Specification of FUTEK Rotary Torque Sensor

PERFORMANCE	
Nonlinearity	±0.2% of RO
Hysteresis	10.1% of RO
Non-repeatability	±0.2% of RO
Rotational Speed	3000 RPM Max
ELECTRICAL	
Rated Output (RO)	2 mV/V nom
Excitation (VDC or VAC)	11 max
Bridge Resistance	350 ohm nom
Connection	10 Pin Bendix PT02A-12-10P
MECHANICAL	
Safe Overload	150% of RO
Material	Aluminum (Housing), Steel Alloy (Shaft)
IP Rating	1P40

2.2 Design of the System

The add-on system is precisely designed to fit onto the EXETER S2T2 traction machine. All the electronic sensors are mounted on the top of the mounting frame, which is installed on the traction machine. The Futek torque sensor and DC motor are connected through the vertical shaft that attaches to the dummy shoe holder at the base frame. The weight was placed on the supporting plate, which was connected to the vertical shaft. Athletic shoes and playing surfaces are subjected to structural loads using dummy shoe holders as shown in Fig. 7.

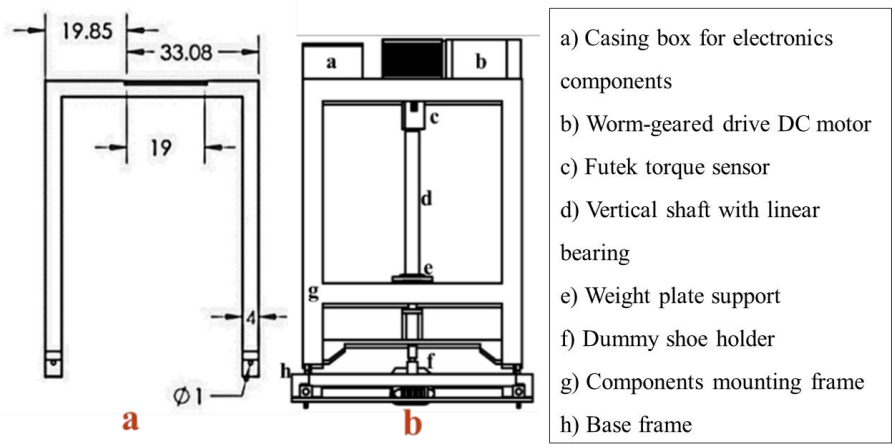

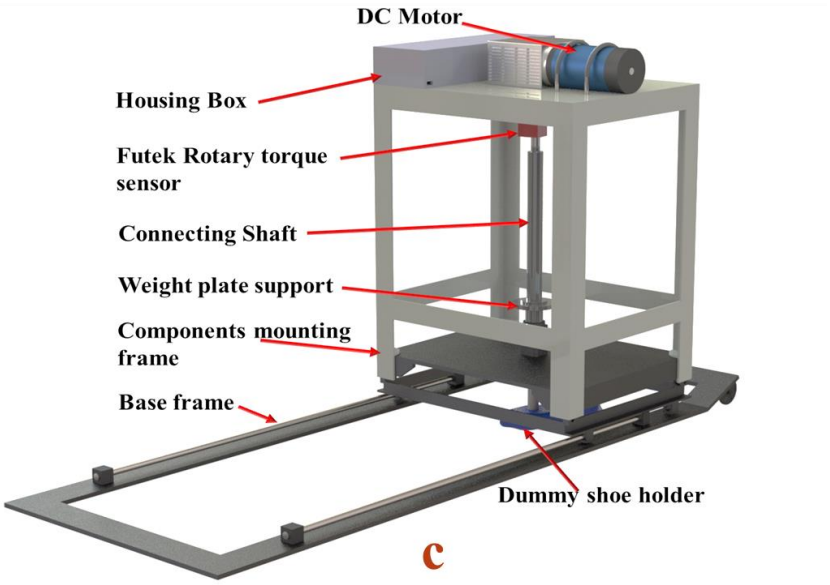

Figure 7. The add-on system's a) drawing with dimensions (cm), b) front view, and c) isometric view

2.3 Fabrication of the System

2.3.1 Manufacturing of Components

Two aspects of the add-on design require consideration for material selection. It is required to provide materials for the fitting mechanism, which is the frame in addition to the housing system. The frame for the add-on system was locally made, and mild steel was used in the mechanical engineering workshop for such structures. For the housing of the electronic system, acrylic materials were used for wire management due to their features such as lightweight, robustness, and weather-resistant thermoplastic that is dimensionally stable, break-resistant, and easily fabricated and glued. The frame was entirely constructed to accommodate the EXETER S2T2 traction machine as a table add-on, utilizing mild steel material and precise measurements to ensure that it did not exceed the required size. For aesthetic appearance, the frame was coated with a dark grey spray. When the frame was finished, it was ready for other components to be added. The DC motor was installed on the frame with the gearbox on top of a hole in

the frame, allowing access to the hexagonal rod from the EXETER S2T2 traction machine. For safety, the motor was secured using open enclosures and M8 bolts, washers, and nuts. After fixing the motor, the next step was to manufacture the coupler to fit the FUTEK rotary torque sensor and attach it to the gearbox so that the rotary sensor can be connected to the gearbox's rotating shaft to transmit the power and also provide proper alignments to the sensor and shaft as shown in Fig. 8(a). Following this, a shaft of comparable height to the FUTEK rotary sensor was manufactured to take its place anytime the torque sensor was not required, so making it a replacement part that keeps the system running independently. Furthermore, an adapter was created with one end to fit the 13/16-inch hexagonal shaft of the EXETER S2T2 traction machine, and the other end to fit the shaft or the FUTEK rotary sensor, both of which had the same square design. Finally, all of the dimensions were carefully chosen to accommodate the available space between the gearbox and the hexagonal rod as shown in Fig. 8(b).

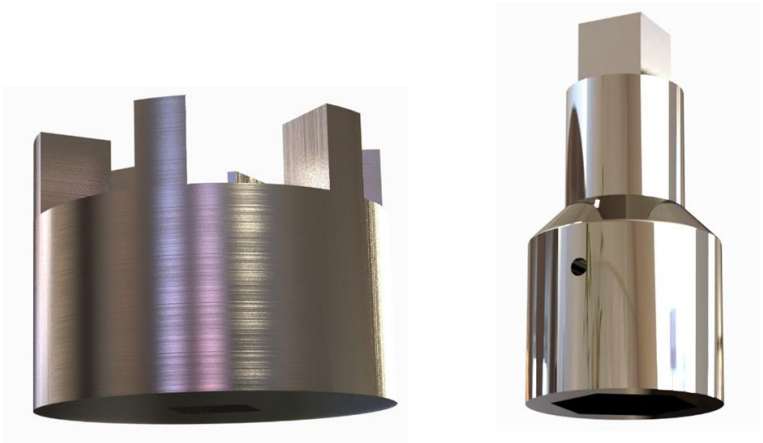

Figure 8. (a) Coupler and (b) Adapter to connect rotary sensor of the traction machine

After all the components were manufactured according to the precise dimensions and specifications, all the parts were then installed in the add-on frame as shown in Fig. 9.

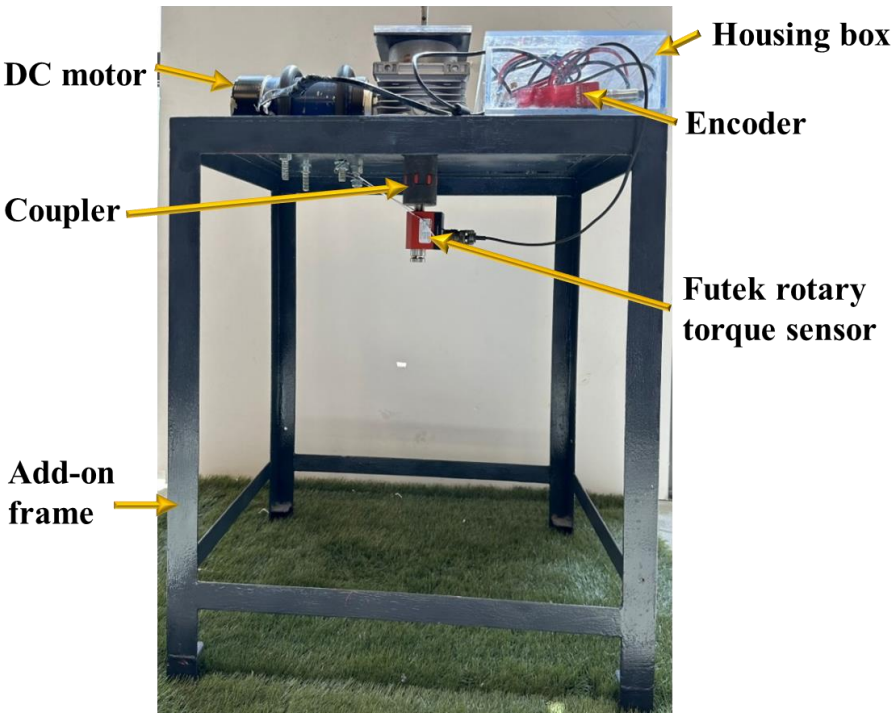

Figure 9. Add-on frame with all installed parts

2.3.2 Assembly of the Traction Machine

The designed mechanical components of the add-on system that was built, were then assembled to verify for dimensional fit. Every component was fitted properly and also the FUTEK sensor and shaft could be removed easily when not required. Afterward, assembled components were integrated with the electronic interface in the mechanical workshop for preliminary laboratory testing and refinement. A SyRen 50A regenerative motor controller from Dimension Engineering [36], the Arduino Duemilanove platform, and an AC-to-DC converter device were utilized to provide the electronic interface for the add-on system. The torque and angle sensors were linked to a worm-geared drive DC motor, which is connected to a vertical shaft that passes through the weight loading plate and is joined to a dummy shoe holder. The shoes compared were fitted to the dummy shoe holder for testing purposes as presented in Fig. 10(a). Fig. 10(b), shows the assembly created beneath the table frame to connect the various components as described.

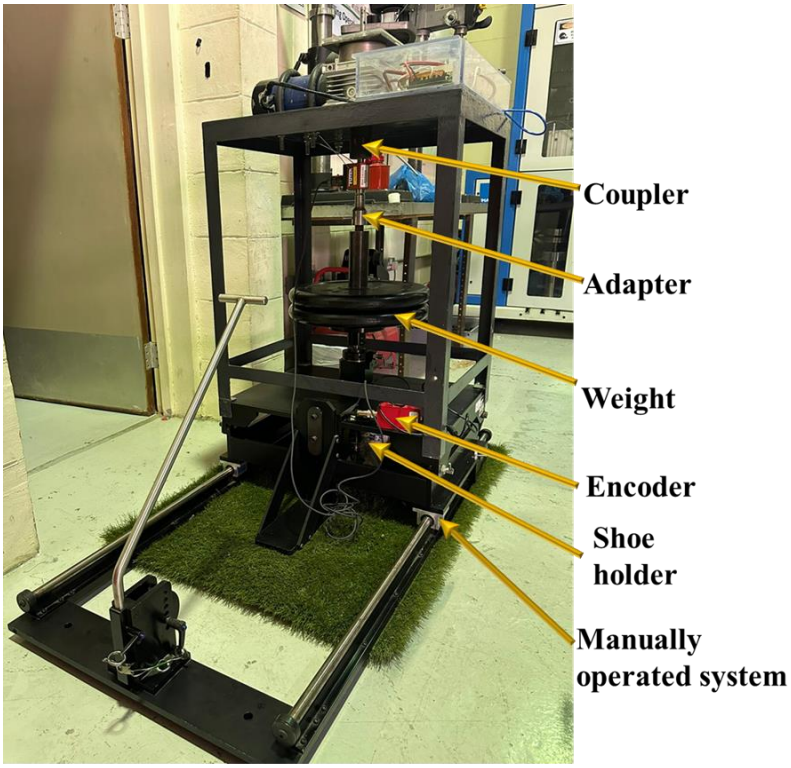

(a)

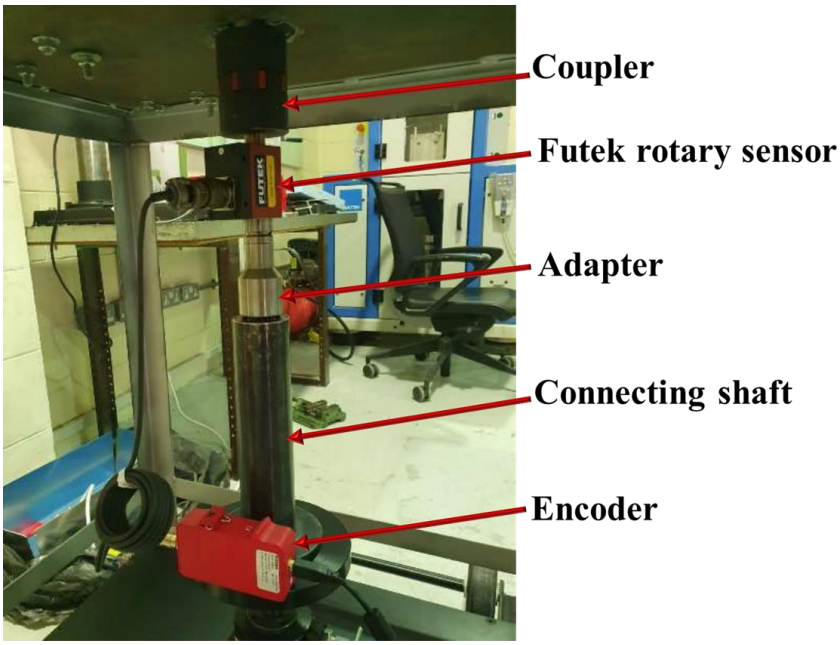

(b)

Figure 10. An overview of automated traction machine

2.4 Testing of the System

The testing of a traction system for measuring the traction of shoes and playing ground involves evaluating the accuracy and reliability of the system in measuring the traction

provided by the shoes and the surface they are used on. This can include workshop tests as well as real-world tests. Some key factors to be considered in the testing process include:

- Versatility: The system should have the ability to adapt and function effectively in a variety of different situations. It should also be capable of measuring traction under various loads and speeds. It will enable accurate and reliable measurements in a wide range of applications and scenarios.
- Sensitivity: The system should be able to accurately measure small changes in traction.
- Repeatability: The system should produce consistent results each time it is used.
- Calibration: The system should be properly calibrated to ensure accurate results.
- Environmental factors: The system should be able to function accurately in different conditions such as varying temperatures, humidity levels, and other environmental factors.
- User-friendliness: The system should be easy to use and provide clear and concise results.

Testing of the traction system can also involve comparing its results to those obtained from other methods to validate its accuracy. It is important to thoroughly test the system to ensure it meets the desired specifications and can be used effectively in different applications. Initially, a test for rotation of the system as a whole was performed. The limit switches were then tested, allowing the machine to rotate according to the coding for just 90 degrees before stopping, with the associated rotational angle measurements. The FUTEK rotary torque sensor was then integrated into the system, and a test was performed to monitor the sensor's output with torque, rotational speed, and angle of rotation.

CHAPTER 3: ENGINEERING DESIGN AND ANALYSIS

3.1 Stress Analysis (Von Mises)

Von Mises stress analysis is a method used in engineering and materials science to predict the failure of a material subjected to complex loading conditions. A stress study was carried out using SolidWorks software as shown in Fig. 11. The weight of the DC motor, which is around 17.0 kg, multiplied by gravitational acceleration results in a force of about 170 N applied to the frame in the simulation. In order to operate the system in extreme working conditions, the torque was adjusted to be the maximum value the motor can provide, which is 150 N.m. The maximum force obtained after the combination of the motor weight and torque was applied for the stress analysis of the frame.

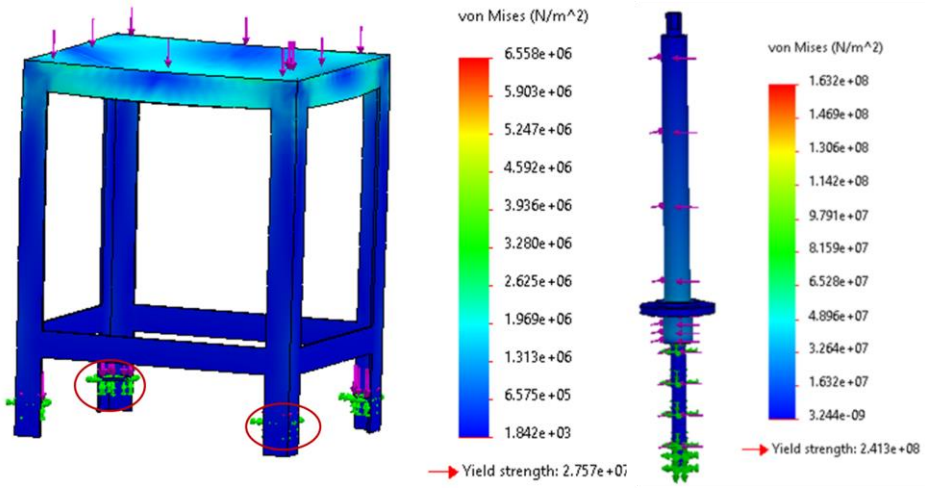

Figure 11. Stress analysis simulation of frame and shaft

In SolidWorks, the boundary conditions for stress analysis are utilized to constrain the component throughout the simulation process to accurately simulate the real-world behavior of the model. The boundary conditions for stress analysis (Von Mises) in SolidWorks include.

1) Fixed constraint: This boundary condition restricts the part from moving in a

certain direction.

2) Concentrated load: A point load is applied to a specific spot on a part by this boundary condition. It simulates the impact of a force operating on a specific location.
3) Distribution load: This boundary condition applies a load over the surface of the part. It is used to simulate the impact of a distributed force, such as weight or pressure.

The obtained value of yield strength through stress analysis is 2.757×10^7 N/m^2 and 3.413×10^8 N/m^2 at the fixed position of the frame and for the shaft respectively as shown in the four legs of the table in Fig. 11. The results of the analysis were used to determine that the system is designed to withstand the applied forces and torques without failure or deformation. In this context, the yield strength determined by stress analysis is 2.757×10^7 N/m^2 and 3.413×10^8 N/m^2 for the frame and shaft. This indicates that if the stress on the material being studied is equal to or greater than this value, it will begin to deform plastically and will not return to its original shape when the load has been removed. It is essential to keep in mind that the yield strength determined by stress analysis is estimated based on the assumptions and parameters used during the simulation. Actual yield strength may vary depending on factors such as manufacturing techniques, material composition, and other environmental factors. Overall, the stress analysis provides useful data about the behavior of the system under extreme loading conditions and can help make certain that it was designed to meet the essential safety requirements. The manufactured system was tested in real-time with the applied load during the torque testing process on the field and shows no vibration or deformation in the frame which validates the results obtained through simulation analysis.

3.2 Factor of Safety Analysis (FoS)

A Factor of Safety (FoS) is a ratio that compares the maximum stress that a material can bear before failure to the load applied. The factor of Safety (FoS) was measured with Finite Element Analysis (FEA) using SolidWorks software for the manufactured frame to know if it can hold the weight of the motor and applied torque as presented in Fig. 12. FoS analysis is a widely used method in engineering to ensure the safety and reliability of structures. FEA involves dividing a structure or component into small elements, analyzing the behavior of each element under different loads, and then combining the results to determine the overall behavior of the structure. The condition of Von Mises stress previously obtained was used to calculate the factor of safety for the manufactured frame and shaft.

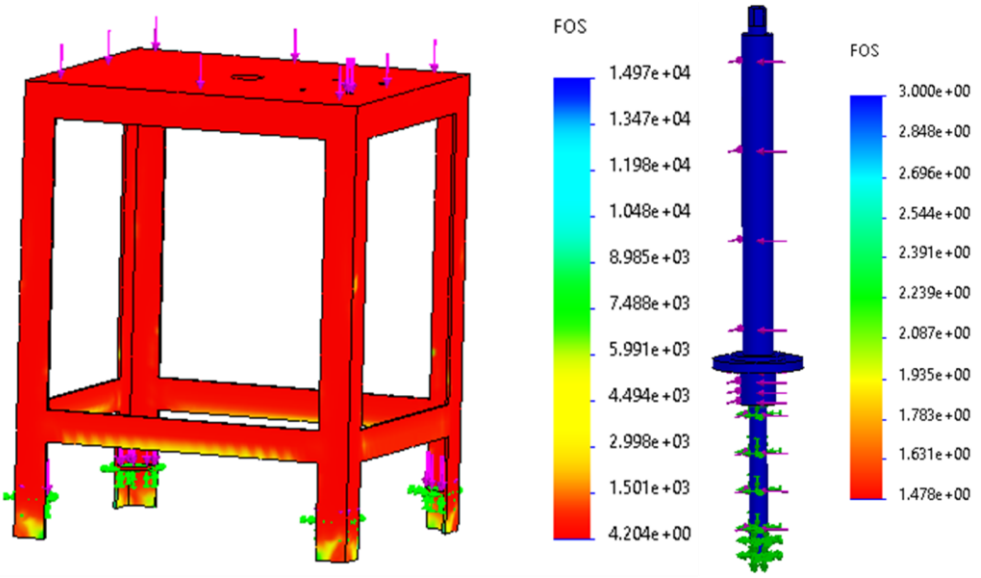

Figure 12. Factor of safety simulation of frame and shaft

The analysis results show the minimum Factor of safety of the designed frame is 4.2, and 1.5 for the shaft, which indicates that the developed frame as well as the shaft can sustain a stress or load that is 4.2 and 1.5 times more than the maximum stress estimated in its intended application respectively. In other words, under typical operating

conditions, the designed frame has a substantial margin of safety and is highly unlikely to fail.

3.2 Fatigue Analysis

Fatigue analysis is useful in manufacturing because it ensures the durability and reliability of the components under continuous loading situations. The stresses and strains that arise during cyclic loading are calculated and used to determine the material's fatigue life and damage percentage over time. Fatigue analysis was done for the developed add-on shaft with the same parameters and data obtained from stress analysis and factor of safety to evaluate the fatigue life of the structure. The results obtained from fatigue analysis show that the failure of the structure is unlikely to occur according to the applied load and torque on the system.

Fatigue analysis simulation results include:

1) Prediction of fatigue life: The predicts the structure's estimated lifetime under cyclic loading parameters.
2) Failure analysis: This assessment identifies significant failure or damaged areas in the components.
3) Damage aggregation: This estimates the amount of damage that accumulates over time as a result of cyclic loading.

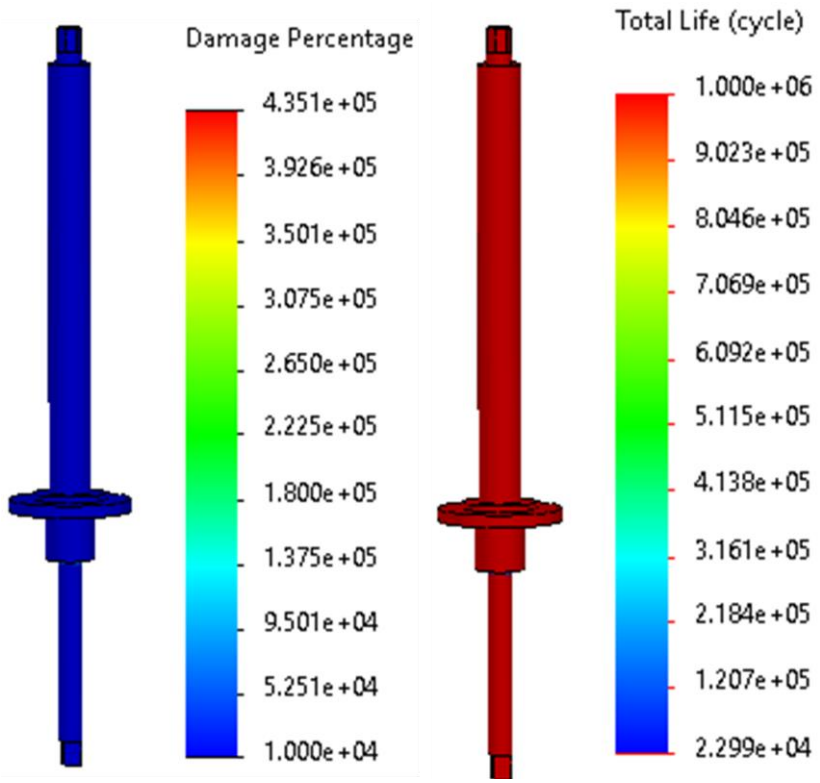

Figure 13. Fatigue analysis simulation

This result shows the total life of the structure is 1.0×10^6 cycles which confirms the safe operation of the manufactured system as shown in Fig. 13, for fatigue analysis simulation. Overall, fatigue analysis simulation results provide valuable insights into the performance and lifespan of a component under cyclic loading conditions.

CHAPTER 4: SOFTWARE DEVELOPMENT

4.1 Development of Arduino program for motor control

The software was developed in accordance with the testing protocol to operate the DC motor with a motor controller (SyRen 50A). An Arduino Duemilanove platform was used to create and run the code for the three pushbuttons to control the DC motor as one for the power button and others for rotation clockwise and anticlockwise of the motor and for two limit switches to restrict the rotation of the motor after hitting the limit switches at 90^{o} on both directions. The motor speed set at SR.motor(127) (baud rate 9600, for SyRen 50A) to rotate the motor at full power as specified full speed of utilized DC motor is 30 rpm, and torque 150 N. By changing the polarity and value SR.motor(-106), the rotation direction and speed of the motor can be changed respectively as shown in Fig. 14. To operate the motor and receive input from limit switches and push buttons, as shown in Fig. 15, the program employs digital and analog pins on the Arduino platform. The angular movement of the motor was restricted with the help of two limit switches placed at 90^{o} to each other and direction was controlled by pushbuttons. The working principle of the Arduino program has been displayed in Fig. 16, as a flow chart.

Figure 14. Developed Arduino program code for the motor control

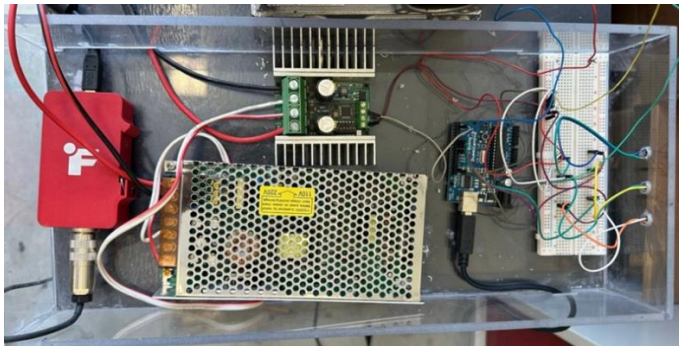

Figure 15. The electronic interface of the add-on system

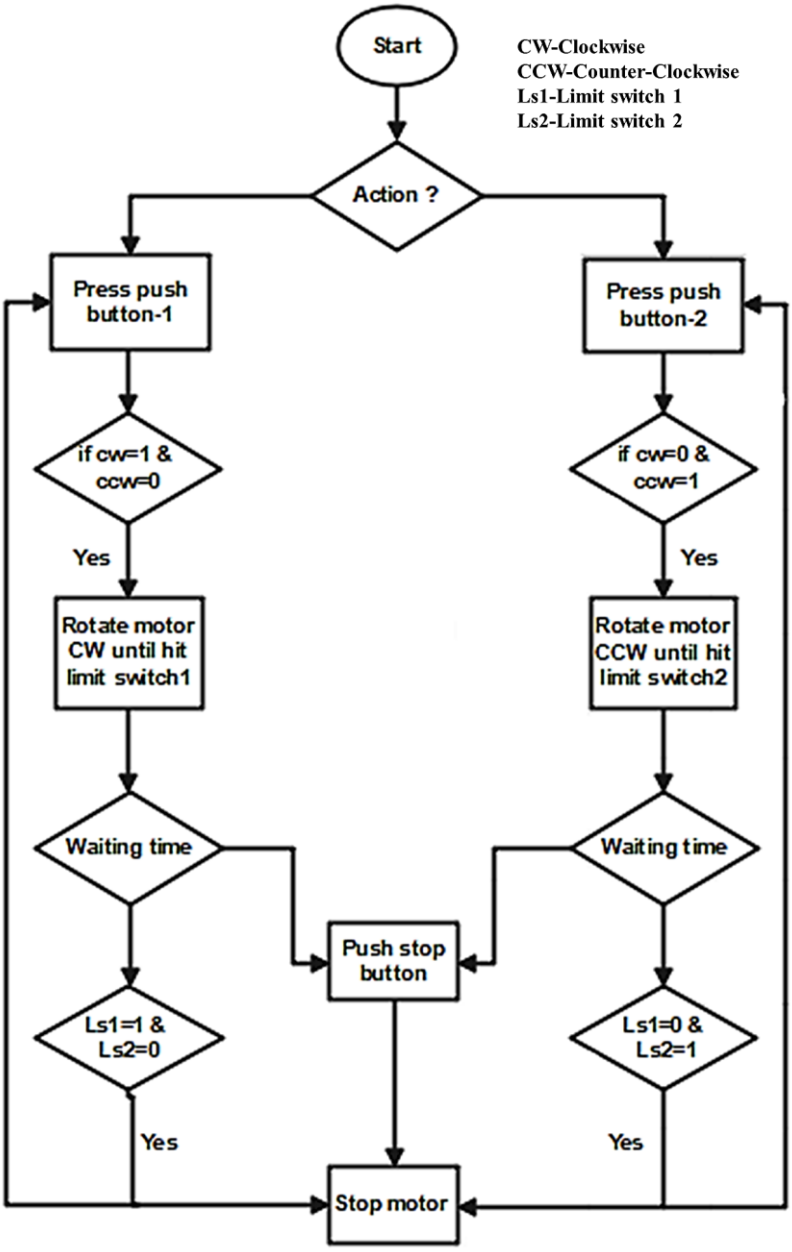

Figure 16. Flow chart of control of motor rotation

4.2 Software and Hardware Interface

The prototype development was divided into two parts. First, there are mechanical components such as the frame, gears, shaft, and adapter that require selection, design, and assembly. Then there were the electrical components, which comprised the Arduino board, a DC motor driver (SyRen 50A), and two limit switches and wires. Furthermore, the inclusion of the FUTEK rotational torque-angle sensor classifies it as a component of the prototype. The assembly and mounting of the whole system on the EXETER S2T2 traction machine are depicted in Fig. 10. On the other hand, for the software interface, serial communications primarily serve as a means for the Arduino board to communicate with any computer or other device. Serial communications require both hardware and software to be implemented. Lines of code are sent to an external extension by the program. The extension transforms the lines of code between Arduino and the device it is controlling into electrical signals and vice versa. A complete schematic of the mechatronic system is shown in Fig. 17.

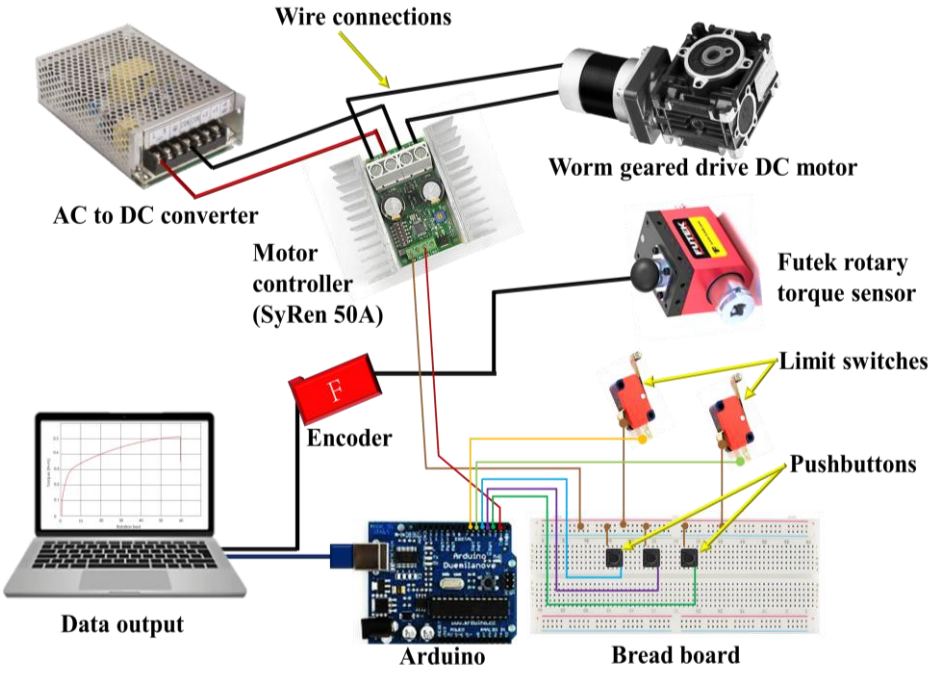

Figure 17. Diagram of electronics connections of Add-on system

The working descriptions of the used components are as follows:

1) AC to DC converter: This was used to convert AC input waveform into pulsating DC output due to the supply of power required for the DC motor.
2) Motor controller: A motor controller (SyRen 50A) is used to control the speed, torque, and direction of an electric motor. The controller's function includes speed control, torque control, direction control, overload control as well as feedback control.
3) Worm-geared drive DC motor: This motor was used to rotate the shaft connected to the dummy shoe holder. It is preferred over other types of motors because of their efficiency, durability, and reliability.
4) Futek rotary sensor: It was used to detect the twisting force (torque) applied to a rotating shaft and convert it into an electrical signal.
5) Encoder: An encoder is a device that is used for rotary sensors to convert rotary motion into digital signals that can be read and interpreted by a microcontroller or other electronic device.
6) Arduino platform: It consists of a microcontroller board and a software development environment to write and upload code to control electronic components such as motors, actuators, sensors, and displays.
7) Limit switch: A limit switch is an electromechanical device that is used to detect the end of the movement of the motor arm. It consists of a mechanical actuator that is connected to a set of electrical contacts, which open or close depending on the position of the actuator.

CHAPTER 5: RESULT AND DISCUSSION

5.1 Shoes and surfaces used for testing

The traction was measured by using the developed add-on system installed on EXETER S2T2 traction machine. This system has two moving components translation as well as rotational which allow the measurement of translation traction and rotational traction at a specific time. It comprises a dummy footform component of various sizes, to which shoes are attached and angled at 20˚ of plantar flexion as can be seen in Fig. 18(b). This configuration is intended to ensure that only the forefoot studs of the shoes come in contact with the surface as shown in Fig.18(c), as described in previous research [17], [18], [29].

Figure 18. Fitted shoe on dummy shoe holder at 20º of plantar flexion

This is to ensure the vertical loads were applied through the shoes onto the playing surfaces with the help of a floating foot-mass component. A Nike (Tiempo) shoe with its outsole and stud as shown in Fig. 19, was used for the traction testing in this research work. The traction was measured on the two playing surfaces artificial and natural grass for the comparison of the traction generated, ability, and performance of the developed system.

Figure 19. Nike (Tiempo) shoe with stud and outsole tested model

5.2 Traction Testing for Shoe-surface

Traction testing for shoe-surface is a method for determining a shoe's slip resistance or rotational resistance on specified surfaces. Different surfaces will have different traction, so it's important to test shoes on a variety of surfaces, including natural grass as well as artificial grass. To ensure accurate readings, the traction machine was calibrated before performing a traction test. After the calibration was done the obtained data were compared with the achieved data of the manually operated system with a torque wrench as shown in Fig. 20, for the similarities in generated results of the torque as shown in Table 3.

Figure 20. Torque wrench used for manually operated traction machine

Table 3. Similarities in traction (peak values) are obtained through manually operated as well as automated systems.

Traction machine	Traction (Peak value) (Nm)		Grass type		Reference
Manually operated	33.7,	34.4	AG,	NG	[37]
Automated operated	31.36	32.44	AG	NG	

To measure the torque generated between artificial and natural grass by applying various normal loads and with different speeds of rotation. The rotational speed was determined based on the extreme condition operation of the developed system in order to utilize its full potential of 150 N torque generation by the DC motor at 30 rpm, as previously indicated. Afterward, the system was tested for other speeds of rotation as 25 rpm with various loads such as 539 N and 588 N. The loads here are chosen to keep in mind the approximation of the athlete's weight to evaluate the proper traction between shoes and playing surfaces to avoid lower extremities injuries. The real-time test results were obtained using Futek rotary torque sensor with an encoder and the data were stored in the output device in an Excel file for post-processing. The real-time data plot of torque-time, power-time, angle-time, and speed time is shown in Fig. 21. The obtained data also plotted with torque against time in an Excel sheet from where all the peak values of the traction were taken for the post-evaluation and validation of the results as displayed in Fig. 22.

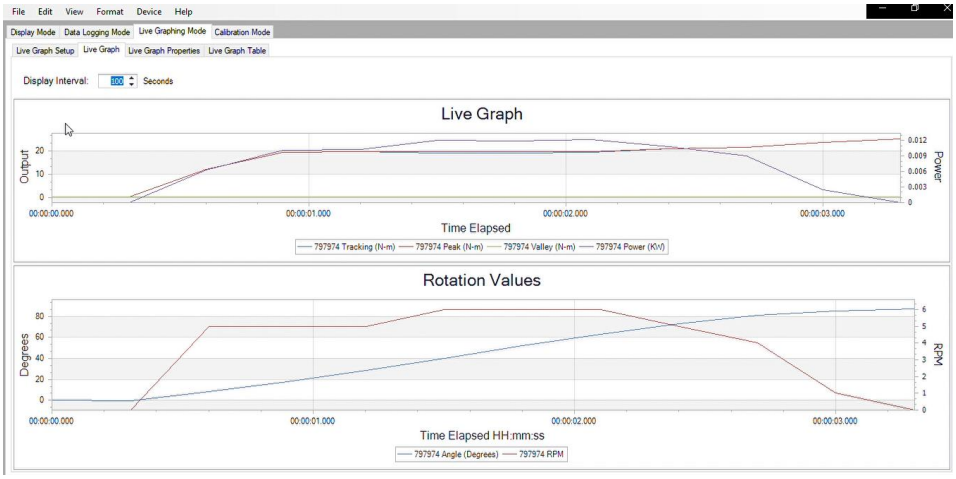

Figure 21. Real-time data plot in Futek rotary torque sensor application

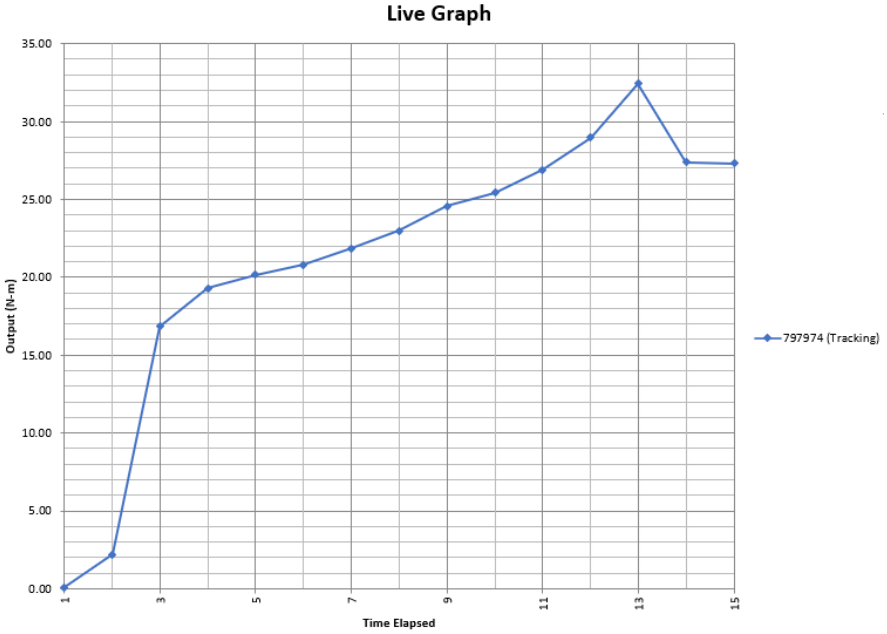

Figure 22. Real-time data Plot for torque vs time

5.3 Experimental data analysis

The analysis of experimental data is an important part of the research process because it helps researchers to derive meaningful conclusions from their experiments and make evidence-based decisions. The experimental data generated through various test processes were collected, analyzed, and interpreted employing several steps such as data preparation, exploratory data analysis, and reporting.

1) Data preparation: This includes arranging and collecting the information to ensure its completeness and precision. Finding and resolving missing data, outliers, and errors in the testing process.
2) Exploratory data analysis: This phase comprises and evaluates the data to understand its characteristics, such as distribution, internal consistency, and variability. It may include generating graphs, tables, and other representations to aid in the identification of patterns and trends in the data.
3) Reporting: This step comprises expressing the analyzed results straightforwardly and understandably. This could include writing a report or making a presentation.

The collected data of rotational torque through various experiments using vertical loads of 539 N and 588 N in a combination of 25 rpm and 30 rpm speeds of rotation were analyzed and evaluated. The rotational curve was plotted against an angular movement of 90^{o} for the two different types of grasses such as artificial and natural grass. The test was performed at a particular load and speed of rotation in outward and inward rotation of the foot on the surface and obtained torque values were recorded. The test was performed using the vertical load of 539 N and at the rotational speed of 25 rpm on artificial grass (AG) as well as on natural grass (NG). The results show the peak torque of 25.89 Nm was generated at the angle of 85.75^{o} for the inward rotation on the AG is the lowest as compared to the 26.02 Nm at 88^{o} of inward rotation on NG, 26.75 Nm at 84.25^{o} on AG, and 28.43 Nm at 87.75^{o} on NG as shown in Fig. 23.

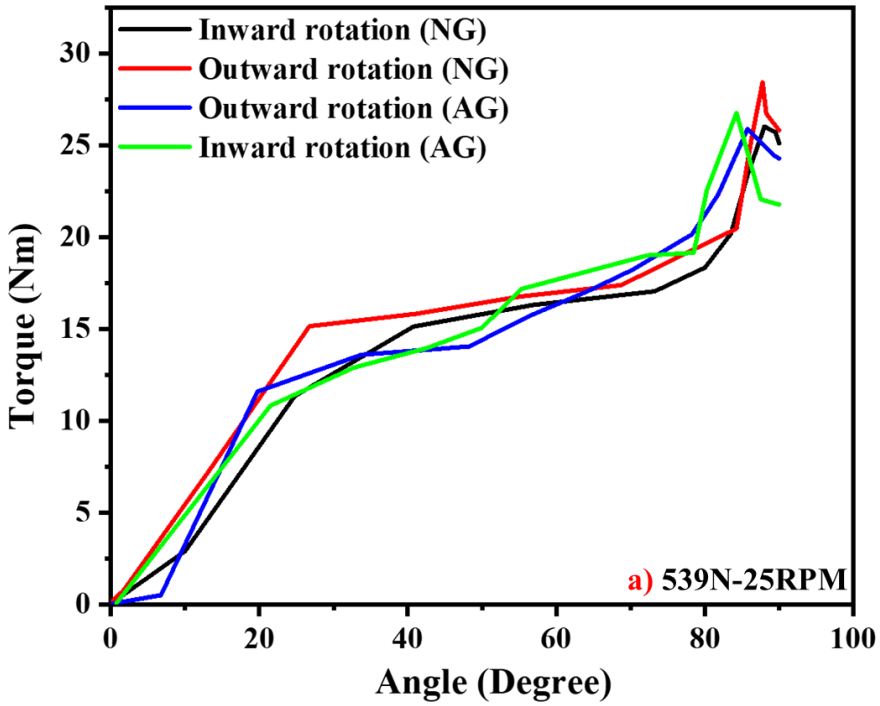

Figure 23. Torque vs angle plot at the load 539 N and speed 25 rpm

Another test was carried out keeping the vertical load 539 N with the rotational speed of 30 rpm and the obtained was analyzed as the finding shows the change in torque value with angle. The lowest torque obtained is 28.44 Nm at an angle of 87.75^{o} for inward rotation on AG, as compared to 29.09 Nm at 86.75^{o} for inward rotation on NG, 29.88 Nm at 84.75^{o} for outward rotation of AG, and 30.86 Nm at 87.25^{o} for outward rotation on NG, as displayed in Fig. 24.

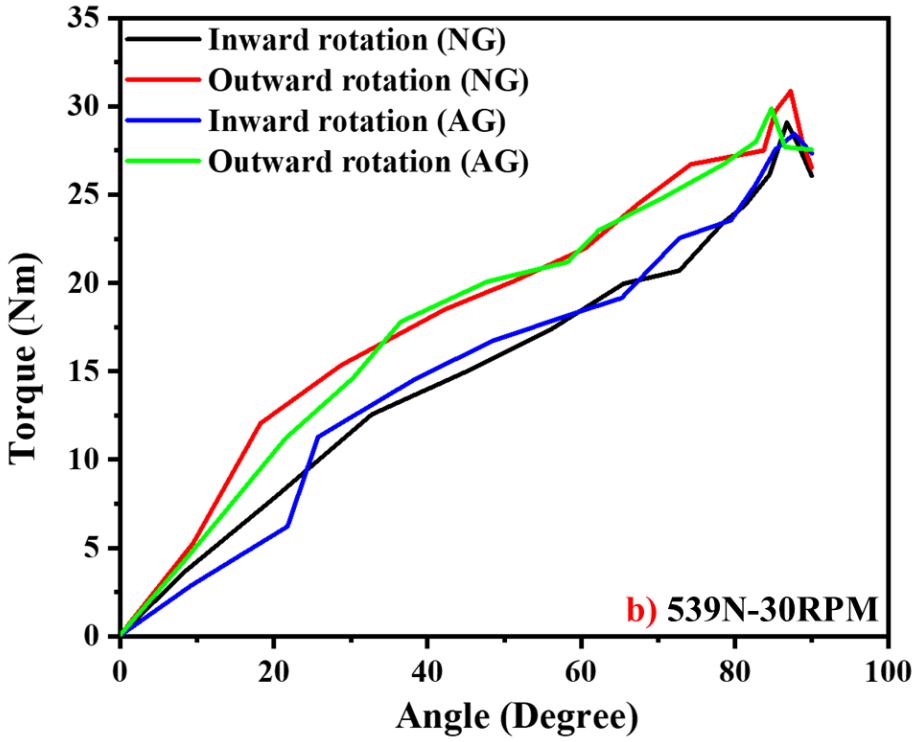

Figure 24.Torque vs angle plot at vertical load 539 N and speed 30 rpm

In this test vertical load increased to 588 N with the speed of rotation at 25 rpm for the evaluation of impact due to load change on the torque generated between shoes and playing surfaces. The outcomes of this experiment were plotted with torque values against an angle of rotation as shown in Fig. 25. The obtained data from this plot was compared and the findings are 28.84 N of torque at 86.25^{o} for inward rotation on AG which is the lowest value amongst the 29.18 N at 88.75^{o} for inward rotation on NG, 30.58 N at 85.25^{o} for outward rotation on AG, and 31.75 N at 87.25^{o} for outward rotation on NG.

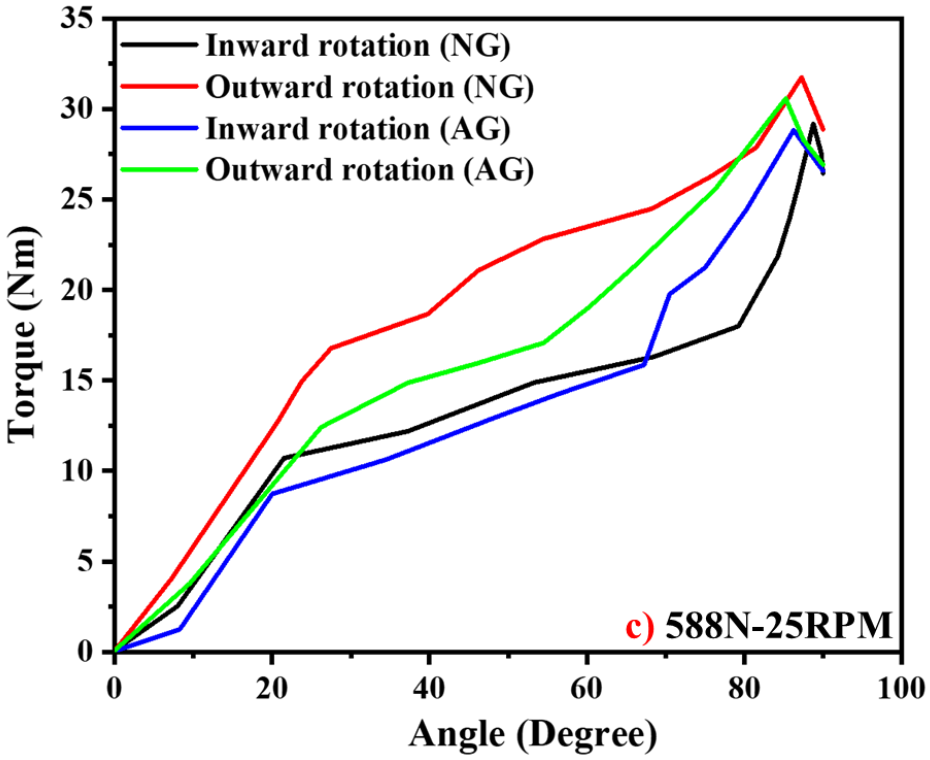

Figure 25. Torque vs angle plot at vertical load 588 N and speed 25 rpm

To have more clarity of the results final tests were done at the vertical load of 588 N and rotational speed of 30 rpm which allows the use of the full capacity of the DC motor at an input torque of 150 N. The obtained torque data from this experiment were analyzed and plotted against the angular movement as presented in Fig. 26. The generated values were compared for a better understanding of the impact of increasing vertical load and speed of rotation on the traction between shoes and surfaces. The maximum torque of 32.44 Nm at an angle of 87.75^{o} was obtained for the outward rotation on the NG, 31.36 Nm at 86.75^{o} for the outward rotation on AG, 30.53 Nm at 85^{o} for the inward rotation on NG, and the lowest torque was for the inward rotation on AG, as 30.42 Nm at 87.5^{o}.

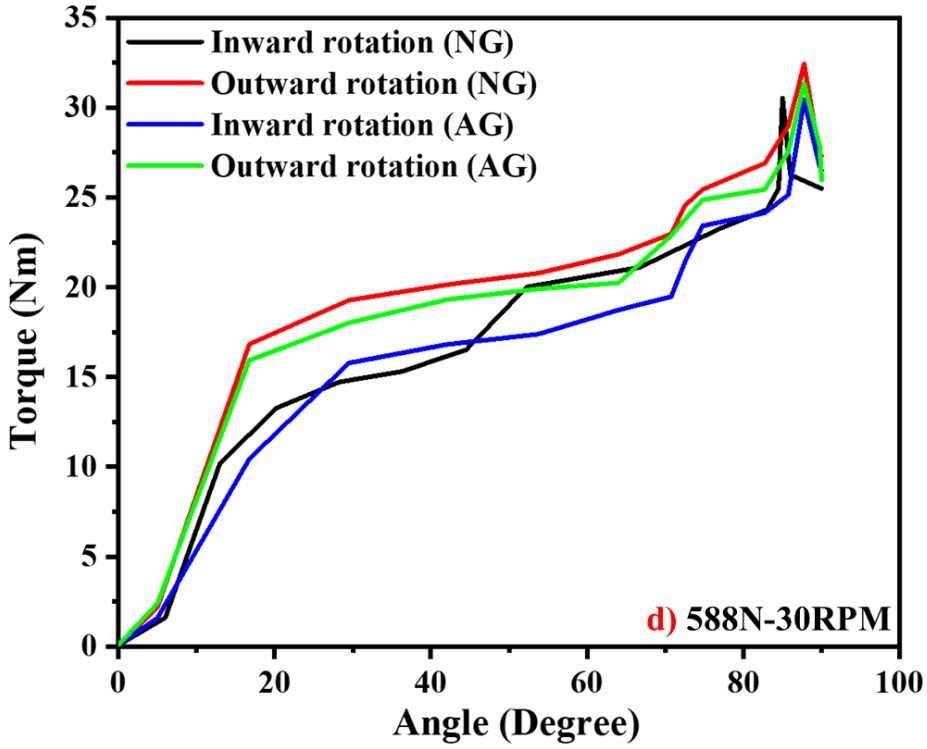

Figure 26. Torque vs angle plot at vertical load 588 N and speed 30 rpm

The obtained peak torque on the playing surface has been verified with the published results in the literature and is aligned with the manually operated system as in previous reports [17], [37].

The test was carried out in both directions of rotation to have a better understanding of the torque generated throughout the testing procedure for inward and outward rotation with different speeds of rotation and vertical loads as previously explained. The outcomes for the tests show the variation in torque generation on artificial and natural grass. At a particular load and speed, the torque generated on the natural grass is higher as compared to the artificial grass but not a significant difference as mentioned in literature [37], [38]. The rotational traction depends on the types of surfaces, shoes, loads, and speed of rotation. Increasing the load or speed of rotation increases the torque between the shoe and the surface. Also, when the speed of rotation or loads decreases the reduction in torque generation has been noticed. The occurrence of peak torque was

noticed in all experiments between 80^{o} to 90^{o}. After the torque reached the peak value further angular movement shows a decrease in torque value.

The behavior of rotational traction also depends on the angle of rotation as can be seen in the plots at a certain angle the value of torque decreased even if the angular movement increased. This is considered a point of inflection where it appears in some cases. This could be due to the occurrence of slipping for a moment between shoes and playing surfaces. Another reason could be the sticking of shoes in the ground.

Overall, the obtained data demonstrate similarities in the change of traction due to variations in loads or rotational speeds. Instead of just peak values, traction can be measured throughout every angular movement.

5.4 Quantitative analysis of data

The study of the results indicates the rotational torque's dependency on various traction testing conditions such as shoe outsole, surface, load, and speed of rotation. In Table 4, a quantitative analysis of obtained data and the change in traction as more traction was generated with higher loads and rotating speed are presented. For natural grass (NG), the highest torque (peak value) is reached with a load of 588 N and a rotational speed of 30 rpm for outward rotation at an angular movement of 87.75^{o,} and the artificial grass (AG) has the lowest torque (peak value) at a load of 539 N and a rotating speed of 25 rpm for inward rotation at an angular movement of 85.75^{o}. These outcomes provide information about the torque angle relationship where at every angular movement a value of torque can be calculated. Increasing the load with the same speed increases the torque produced and increasing the speed with the same load also increases the torque produced between the shoes and surfaces and visa-versa.

Table 4. Rotational torque between shoes, artificial grass (AG), and natural grass (NG) with various loads and speeds of rotation

Load (N)	Speed (rpm)	Rotational Torque(Nm) (Peak value)			
		Inward (AG)	Outward (AG)	Inward (NG)	Outward (NG)
539	25	25.89	26.75	26.02	28.43
539	30	28.44	29.87	29.09	30.86
588	25	28.84	30.58	29.18	31.75
588	30	30.42	31.36	30.53	32.44

5.5 Rotational stiffness

Rotational stiffness is a fundamental property that characterizes the resistance of a system or object to rotational motion when subjected to an applied torque or twisting force. In the context of sports, rotational stiffness (RS) plays a crucial role in providing stability, support, and control during dynamic movements. The ability to change direction, execute quick turns, and maintain balance is directly influenced by the rotational stiffness of the between shoes and playing surfaces. A higher rotational stiffness typically leads to increased stability and control, allowing athletes to perform precise movements with enhanced efficiency.

The rotational stiffness was calculated with the generated torque by using Hooke's Law for rotational systems as shown in equation (1) [39].

$$K = \frac{\Delta T}{\Delta \theta} \tag{1}$$

Where K is rotational stiffness, ΔT is the change in torque, and the change in angular rotation is represented by Δθ. This equation signifies that the torque required to rotate the system is directly proportional to the angular displacement experienced.

A substantial increase and reduction in stiffness have been seen at specific angles, which might be the reason of the athlete's shoes sticking and slipping on the playing surfaces, as shown in Fig. 27. Between angles 0 to 26.75 degrees, the stiffness is

measured to be 32.47 Nm/rad. This indicates a relatively high resistance to rotation for the given torque within this range of angles. As the angle increases to the range of 26.75 to 68.75 degrees, the stiffness decreases to 2.97 Nm/rad. This lower stiffness value suggests a reduced resistance to rotation compared to the previous range. However, a significant shift in stiffness is observed at an angle of 84.25 to 87.75 degrees, where the stiffness jumps to 135.86 Nm/rad. This substantial increase in stiffness implies a substantial resistance to rotation, indicating a change in the mechanical behavior of the system or object at that specific angle range.

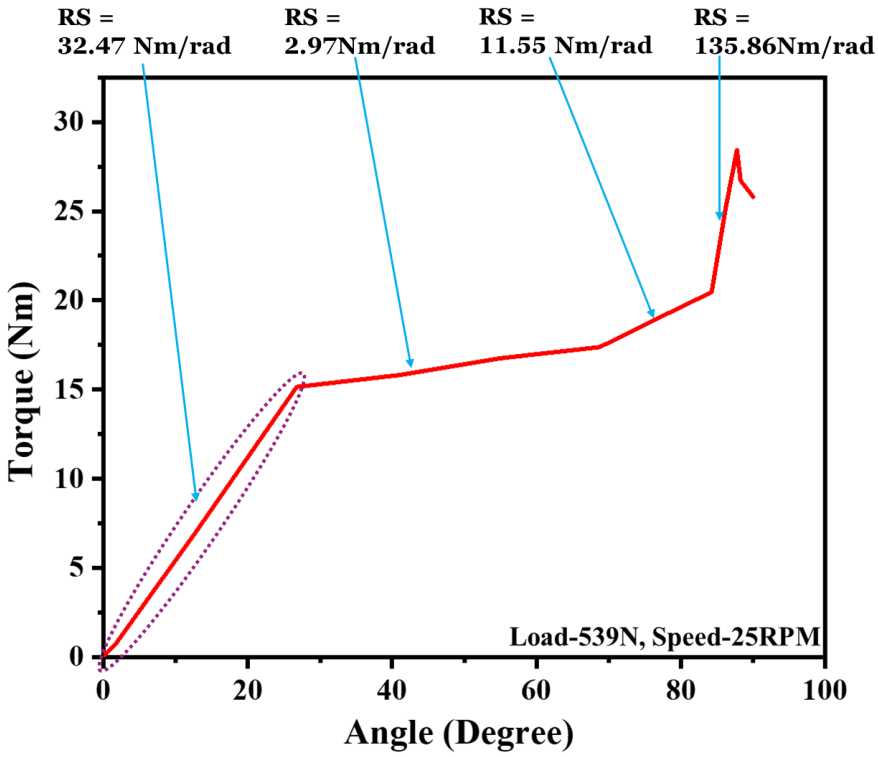

Figure 27. The curve of torque against angle with change in stiffness

CHAPTER 6: NON-LINEAR ROTATIONAL STIFFNESS MODEL

Non-linear Rotational Stiffness models are mathematical representations that describe how materials deform in response to applied forces or stresses. These models assist in understanding and forecasting material characteristics such as elasticity, shear stress, and strain as a function of variables such as shear rate, temperature, and time.

Diverse models have been created to represent the behavior of various materials. The following are some commonly employed numerical models [39]–[41]:

1. Linear Elastic Model: This model implies a linear relationship between torque and angle, based on Hooke's law. It is suitable for materials having completely elastic behavior, which means they flex appropriately to the applied torque with no energy loss.
2. Nonlinear Elastic Model: Modified Bouc-Wen model was used for the more complicated models that can be utilized for materials that demonstrate nonlinear elastic behavior. These models accommodate nonlinearity in the torque-angle connection and can either be empirical or analytical.
3. The Power-Law Model: It is frequently employed for materials that exhibit shear-thinning or shear-thickening behavior. The torque-angle connection in this model follows a power-law relationship, with the torque being a function of the angle raised to a power exponent.
4. The Herschel-Bulkley Model: It is appropriate for materials that exhibit yield behavior, where a particular torque threshold must be surpassed before the material begins to deform. To explain the behavior of the material, this model comprises factors such as yield stress, consistency index, and flow behavior index.

1. The numerical model was developed using results obtained after the testing of the system with a load of 539 N and a speed of rotation at 25 rpm.

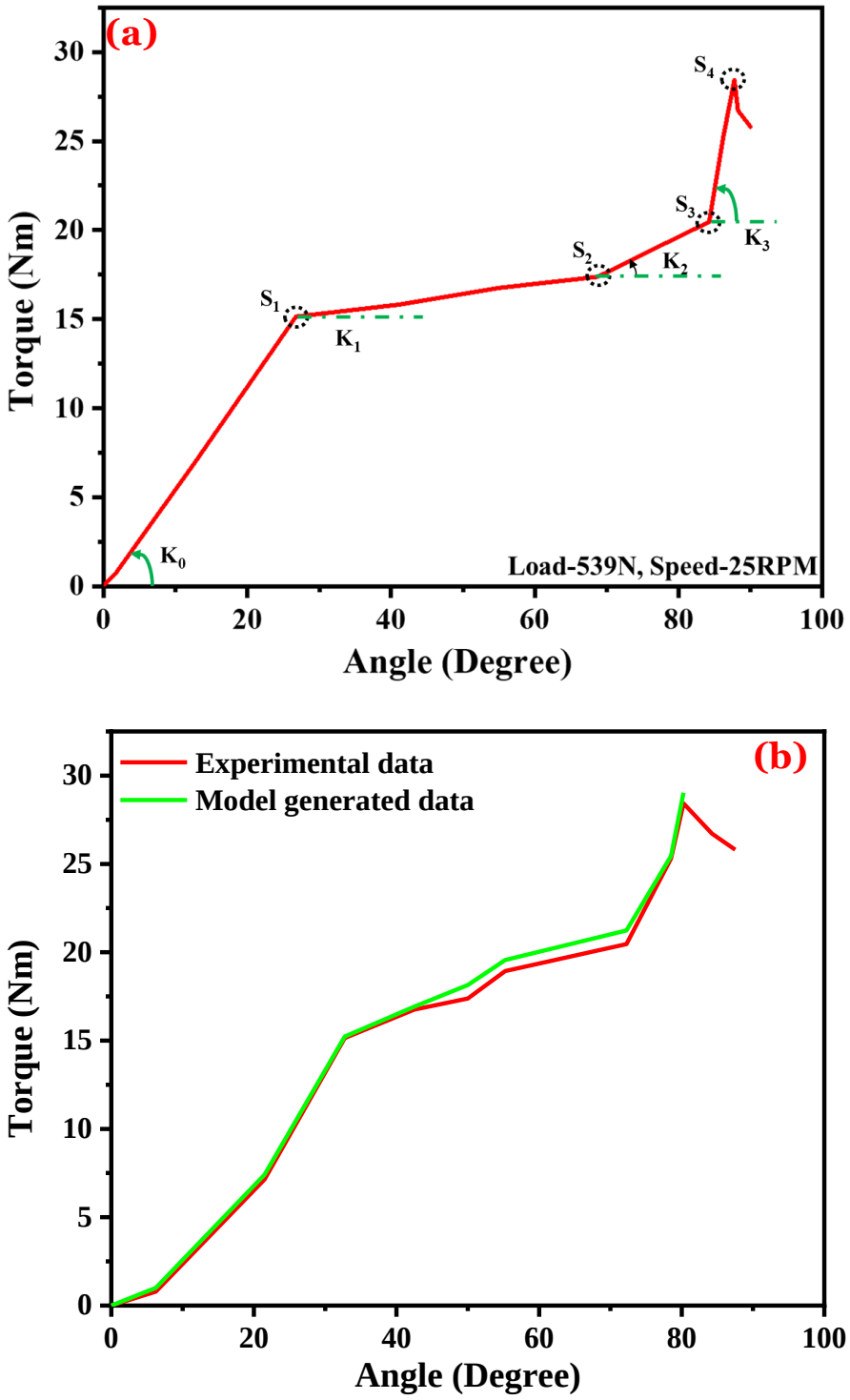

Figure 28. Graphical representation of torque vs angle with (a) real-time test results, (b) real-time data superimposed with model-generated data

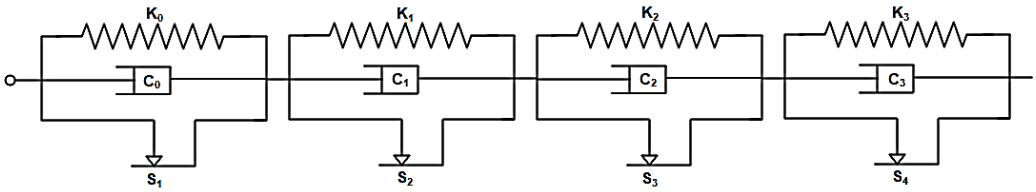

Figure 29. Modified Bouc Wen model with stiffness, slip, and damper

After conducting tests on the traction machine at a rotational speed of 25 rpm and a testing load of 539 N, various parameters were measured to characterize the system's behavior. The torque-angle curve, depicted in Figure 28(a), provided the rotational stiffness values: K_0 = 32.47 Nm/rad, K_1 = 2.98 Nm/rad, K_2 = 11.55 Nm/rad, and K_3 = 135.86 Nm/rad. Additionally, the slip torque values were obtained from the same curve, S_1 = 15.23 Nm, S_2 = 17.42 Nm, S_3 = 20.55 Nm, and S_4 = 28.43 Nm. To calculate the damping coefficient, the angular velocity vs. time curve as displayed in Fig. 30(a) was utilized. From this curve, the damping coefficients were determined as C_0 = 0.036 rad/s^2, C_1 = 0.51 rad/s^2, C_2 = 0.17 rad/s^2, and C_3 = -0.79 rad/s^2. These values were calculated using equations (2) and (3), which were employed to calculate the angular velocity and determine the numerical model as mentioned below [42];

$$\omega = \frac{\Delta\theta}{\Delta t} \tag{2}$$

$$C = \frac{\Delta\omega}{\Delta t} \tag{3}$$

Here, $\Delta\theta$ is the change in rotational angle, Δt is the change in time, ω angular velocity, $\Delta\omega$ is the change in angular velocity and C is for the damping coefficient.

$$T(\theta_t) = C_0\omega + K_0(\theta_t - \theta_0) + K_1(\theta_t - \theta_1) + K_2(\theta_t - \theta_2) + K_3(\theta_t - \theta_3) \tag{4}$$

With the help of equation (4) the modified Bouc-Wen model was generated as represented in Fig. 29, with extra parameters such as damping coefficient C1 and stiffness constant K1, K2 as compared to the Bouc-Wen model [40]. The torque-angle

curve allows for a comparison between real-time data and data obtained from the generated model. In Figure 28(b), the experimental data and the data obtained from the model are superimposed, showing similar results with minimal differences in torque values. This indicates that the traction between shoes and the playing surface can be predicted by considering the angle of rotation, along with other factors such as applied load and rotational speed. The consistent results between the experimental and modeled data demonstrate the model's ability to effectively capture and predict the behavior of the shoe-surface interaction during rotational motions.

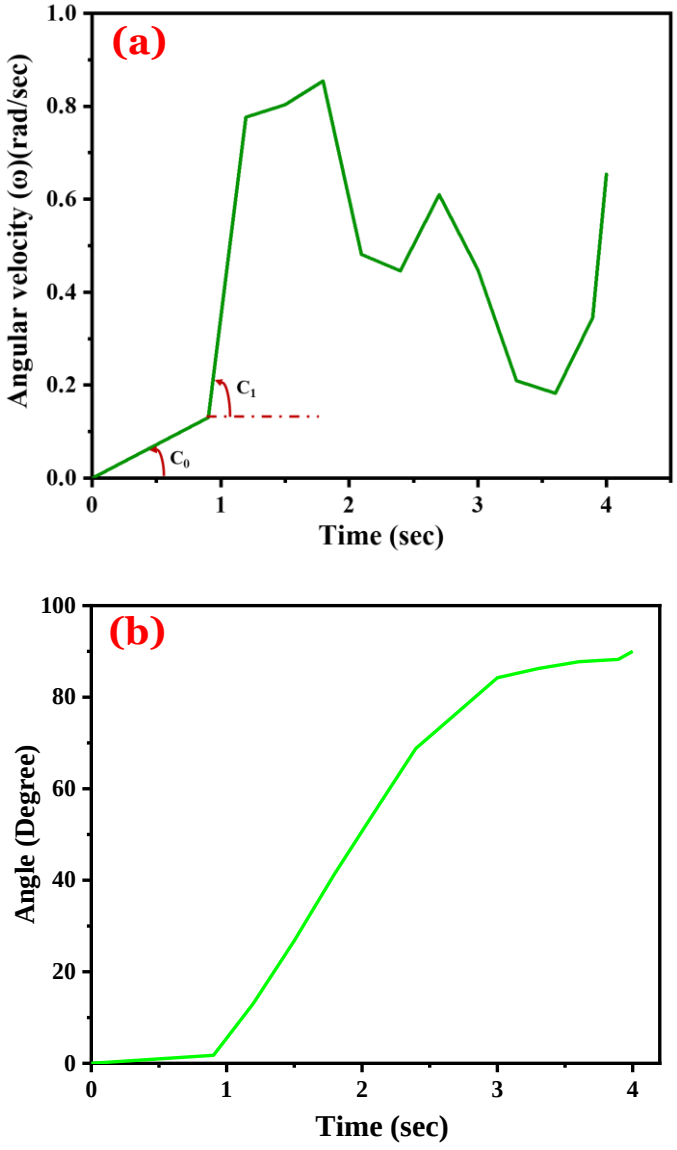

Figure 30. Graphical representation of (a) angular velocity vs time with damping coefficients, and (b) angle vs time curve

Table 5. Calculated values after analysis of data achieved from traction machine test

S. No.	Torque (T) (Nm)	Angle (θ) (rad)	Time (t) (sec)	Angular velocity (ω) (rad/sec)
1	0.795	0.031	0.903	0.130
2	7.148	0.228	1.195	0.776
3	15.142	0.468	1.499	0.803
4	15.823	0.722	1.795	0.854
5	16.752	0.963	2.094	0.481
6	17.382	1.203	2.397	0.446
7	18.931	1.339	2.699	0.610
8	20.458	1.474	3.000	0.449
9	25.306	1.509	3.301	0.210
10	28.428	1.536	3.603	0.183
11	26.719	1.544	3.894	0.345
12	25.805	1.575	4.000	0.654

2. The same approach was utilized to examine the impact of changing the applied load to 588 N while maintaining a rotational speed of 25 rpm.

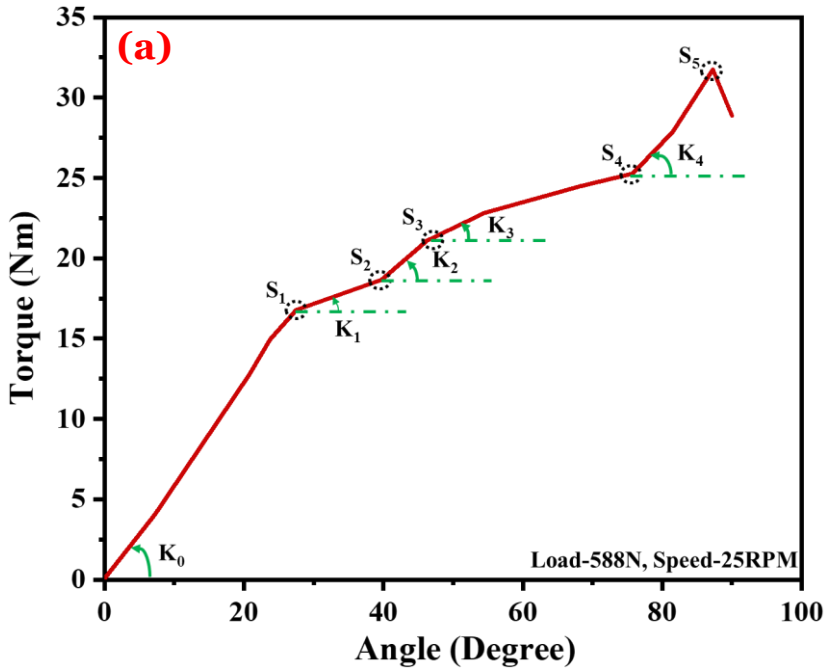

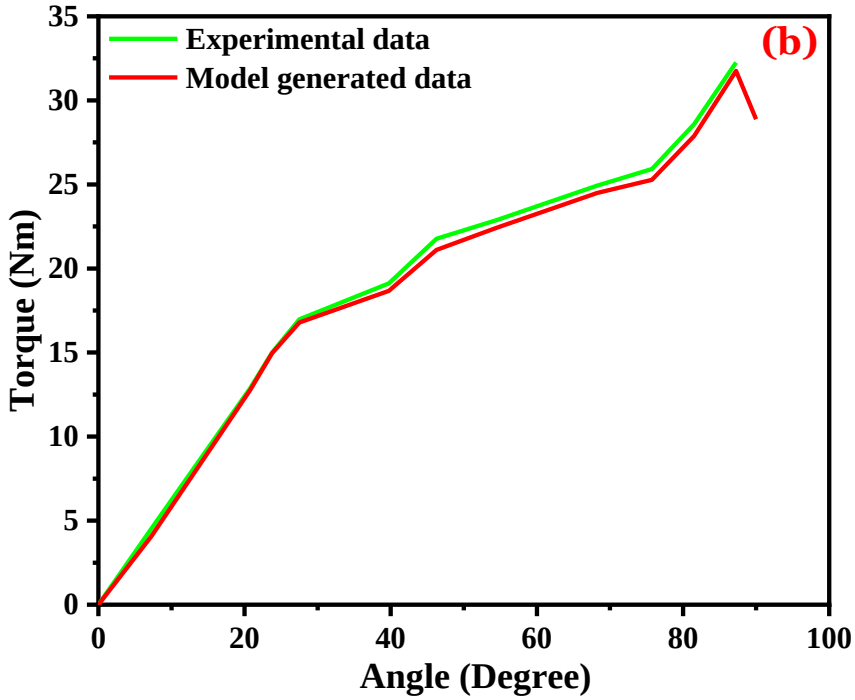

Figure 31. The curve of torque vs angle with (a) experimental data (b) experimental data superimposed with model-generated data

The rotational stiffness values were calculated based on the obtained data from the real-time testing. The results show that the rotational stiffness varies at different angles of rotation. The rotational stiffness values are, K_0 = 35.05 Nm/rad, K_1 = 8.93 Nm/rad, K_2 = 21.24 Nm/rad, K_3 = 8.18 Nm/rad, and K_4 = 32.01 Nm/rad.

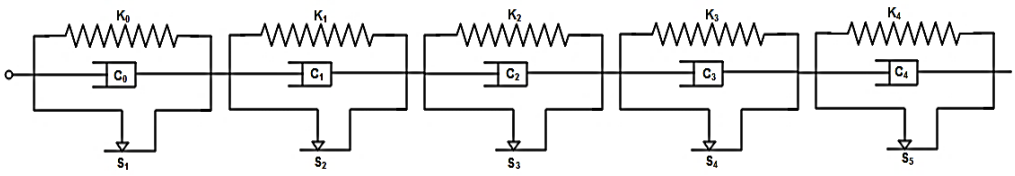

Figure 32. Modified Bouc-Wen model at different testing conditions

Figure 31(a) shows that the stiffness transition is more gradual than in the previous study, where the effect of increasing the testing load was investigated. This shows that the modified equation (5), derived from equation (4), captures stiffness changes more smoothly.

$$T(\theta_t) = C_0\omega + K_0(\theta_t - \theta_0) + K_1(\theta_t - \theta_1) + K_2(\theta_t - \theta_2) + K_3(\theta_t - \theta_3) + K_4(\theta_t - \theta_4) \quad (5)$$

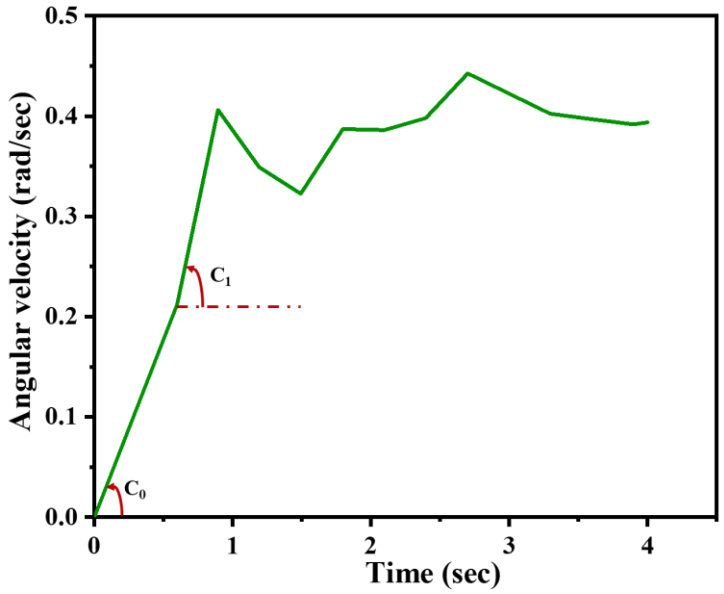

Figure 33. Graphical representation of angular velocity vs time with damping coefficients

The damping coefficient values were obtained from the angular velocity vs time curve analysis. The calculated damping coefficients are C_0 = 0.35 rad/s^2, C1 = 0.66 rad/s^2, C_2 = -0.19 rad/s^2, C_3 = 0.10 rad/s2, and C_4 = -0.04 rad/s^2. These coefficients indicate the level of damping present in the system and its effect on the rotational torque. The generated numerical model takes into account these damping coefficients, resulting in a slight variation in torque values compared to the experimental data. This can be observed in Figure 31 (b), where the torque vs angle curve shows minor deviations due to the additional damping factor introduced in the model. Overall, the developed numerical model can be utilized to calculate the torque between the shoes and the playing surface, allowing for predictions to be made under different conditions.

3. The analysis was done at the testing load of 539 N and changing the speed of rotation to 30 rpm.

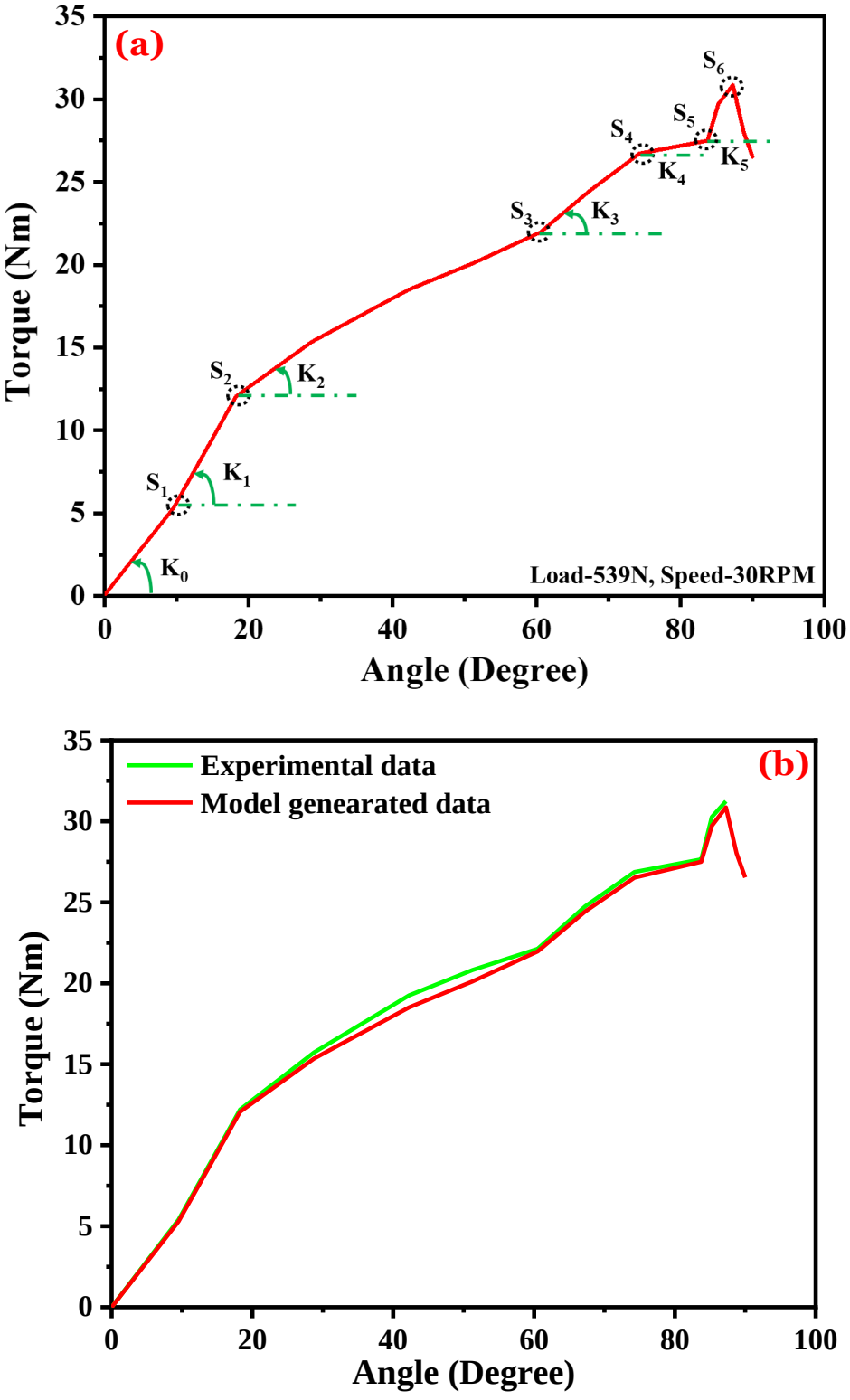

Figure 34. Plot of torque against angle with (a) experimental data (b) experimental data superimposed with model-generated data

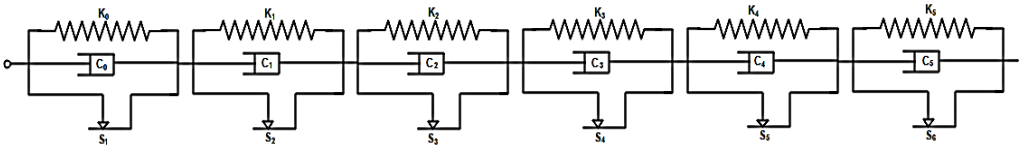

Figure 35. Modified Bouc-Wen model at the different rotational speed

The calculated values for rotational stiffness (K) and slip torque (S) are as K_0 = 31.87 Nm/rad, K_1 = 44.19 Nm/rad, K_2 = 13.39 Nm/rad, K_3 = 19.78 Nm/rad, K_4 = 4.71 Nm/rad, K_5 = 54.81 Nm/rad, S_1 = 5.30 Nm, S_2 = 12.07 Nm, S_3 = 21.96 Nm, S_4 = 26.72 Nm, S_5 = 27.51 Nm, and S_6 = 30.86 Nm. These values represent the stiffness of the system at different angles and the torque required to initiate slipping between the shoe and the playing surface.

$$T(\theta_t) = C_0\omega + K_0(\theta_t - \theta_0) + K_1(\theta_t - \theta_1) + K_2(\theta_t - \theta_2) + K_3(\theta_t - \theta_3) + K_4(\theta_t - \theta_4) + K_5(\theta_t - \theta_5) \quad (6)$$

The torque vs angle curve was analyzed at a testing load of 539 N and a rotational speed of 30 rpm. This analysis allowed for the calculation of rotational stiffness and slip torque, as depicted in Fig. 32 (a). It was observed that the stiffness values exhibited a smooth transition as the speed of rotation increased, while the applied load remained constant. This finding suggests that the speed of rotation has an influence on the system's stiffness, indicating a potential relationship between rotational speed and the traction characteristics of the shoe-surface interaction.

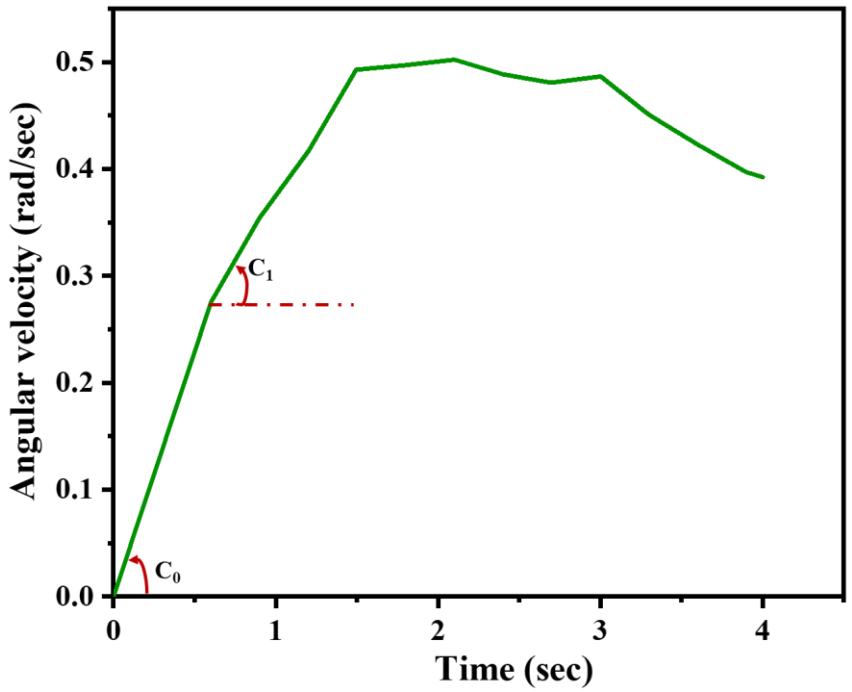

Figure 36. The plot of angular velocity vs time with damping coefficients.

The damping coefficient was determined by analyzing the angular velocity curve, yielding values of C_0 = 0.46 rad/s², C_1 = 0.16 rad/s², C_2 = 0.015 rad/s², C_3 = -0.012 rad/s², C_4 = 0.014 rad/s², and C_5 = -0.094 rad/s². These measurements play a crucial role in developing a numerical model to investigate the behavior of shoe-surface interactions. The rotational stiffness values (K_0, K_1, K_2, K_3) indicate the resistance to the rotation of shoes on the playing surfaces during testing. Higher rotational stiffness values suggest a stiffer surface, providing stability and control during dynamic movements. These stiffness values, along with slip torque and damping coefficients, are essential parameters for the developed numerical model. The numerical models created based on these parameters can be used to predict the torque between shoes and the playing surface under specific conditions, as illustrated in Fig. 28(b), 31(b), and 34(b). Notably, the torque calculated from both real-time tests and numerical models

exhibits similar results, demonstrating the impact of changes in the angle of rotation. This research opens up new possibilities for calculating torque and rotational stiffness between shoes and the playing surface, which contributes to a better understanding of traction-related lower extremity injuries in athletes. Consequently, this knowledge can used for the selection of shoes that are compatible with specific playing surfaces, helping to prevent such injuries.

CHAPTER 7: CONCLUSION AND FUTURE RECOMMENDATION

7.1 Conclusions

In this project, meticulous attention was given to the design and construction of the mechatronic add-on system, which was based on an existing manually operated traction machine. Specific requirements, such as dimensions, component count, fitting precision, height, and weight, were carefully considered to ensure the system met desired specifications. To enable automation, highly reliable and accurate measuring instruments, including the rotary torque/angle sensor and DC motor, were incorporated into the design. The system underwent rigorous testing in real-time applications, showcasing its enhanced capabilities and improved efficiency in the testing process. Notably, the system significantly reduces the time required for data collection and evaluation by employing the instant data generation functionality of the rotary torque/angle sensor. Real-time data can be obtained and visualized through illustrated relation graphs, providing valuable insights into the relationship between torque, angular rotation, rotational speed, and operation time. The system was used to calculate rotational traction between shoes and different types of playing surfaces, such as artificial grass (AG) and natural grass (NG). Interestingly, the results revealed no significant difference in traction between AG and NG under specific load and speed conditions. However, variations in traction were observed between inward and outward rotations, which depended on factors such as load, speed, and the type of grass surface. The main results and outcomes of the thesis can be summarized as follows:

1) A mechatronic system add-on was developed with enhanced functionality. This can be retrofitted.
2) The system allows tedious tasks to be carried out automatically and with less effort from users.

3) The results are more repeatable and accurate and depend less on human interaction.
4) The system can be used to not only get peak torque as common practice to date but also real-time torque and angle. This may lead to a further understanding of traction between shoes and surfaces.
5) The addition of load and speed of rotation can further be studied within a reasonable time.
6) The direction of rotation can also be studied in more depth.
7) One key achievement was in obtaining the rotational stiffness and a new perspective and understanding of traction.
8) A numerical model was developed and used to calculate the torque based on the given parameters which shows similar results.
9) These numerical models provide the prediction of torque at any given angle of rotation without performing an actual test in real-time.
10) The torque (peak value) obtained throughout all experiments are 25.89, 26.75, 26.02, 28.43, 28.44, 29.87, 29.09, 30.86, 28.84, 30.58, 29.18, 31.75, 30.42, 31.36, 30.53, 32.44 Nm.
11) After reaching the peak torque a sudden change (decrease) in torque has been noticed that could be due to the loss of stability of the athletes on the ground which may lead to lower limb injuries.

7.2 Future Recommendation

One of the key advantages of this system is its upgradability, which allows for continual improvement of the system in most aspects. The convenience of collecting and analyzing data is one area in which there is an opportunity to enhance. Currently, data is transmitted from the control units to a portable computer via a wired connection.

However, it is possible to create a mobile application that will make the testing procedure more practical, wireless, and seamless. The manual process of applying vertical loads in the testing procedure can also be upgraded. By utilizing alternative methods such as a hydraulic press, the issues associated with the weight-changing process can be eliminated, resulting in more accurate and efficient measurements. Furthermore, it is recommended to further investigate the effects of rotational speed and direction in relation to injury prevention using the traction measuring system. The newly obtained rotational stiffness values can serve as a basis for generating numerical models that predict torque at specific angles. By conducting additional research on these models, their accuracy and reliability can be improved. Additionally, it is worth considering the implications of observed changes, particularly sudden change in rotational stiffness at certain angles and their potential impact on players. Exploring these aspects in future research would provide valuable insights for optimizing footwear design and playing surface selection to minimize the risk of lower extremity injuries.

REFERENCES

[1] J. Worobets and J. W. Wannop, “Influence of basketball shoe mass, outsole traction, and forefoot bending stiffness on three athletic movements,” *Sport. Biomech.*, 2015, doi: 10.1080/14763141.2015.1084031.

[2] B. Keshvari and V. Senner, “Comparison of shoe-surface tractions on various playing surfaces in futsal,” in *Procedia Engineering*, 2015, vol. 112, pp. 267–272, doi: 10.1016/j.proeng.2015.07.245.

[3] J. Clarke, M. J. Carré, L. Damm, and S. Dixon, “The development of an apparatus to understand the traction developed at the shoe-surface interface in tennis,” *Proc. Inst. Mech. Eng. Part P J. Sport. Eng. Technol.*, vol. 227, no. 3, pp. 149–160, 2013, doi: 10.1177/1754337112469500.

[4] A. Pedroza, S. Fernandez, R. Heidt, and C. Kaeding, “Evaluation of the shoe-surface interaction using an agility maneuver,” *Med. Sci. Sports Exerc.*, vol. 42, no. 9, pp. 1754–1759, 2010, doi: 10.1249/MSS.0b013e3181d7d307.

[5] S. Forrester and P. Fleming, “Traction forces generated during studded boot-surface interactions on third-generation artificial turf: A novel mechanistic perspective,” *Eng. Reports*, vol. 1, no. 5, pp. 1–21, 2019, doi: 10.1002/eng2.12066.

[6] D. De Clercq, G. Debuyck, J. Gerlo, S. Rambour, V. Segers, and I. Van Caekenberghe, “Cutting performance wearing different studded soccer shoes on dry and wet artificial turf,” *Footwear Sci.*, vol. 6, no. 2, pp. 81–87, 2014, doi: 10.1080/19424280.2014.895056.

[7] R. Kent, J. Crandall, J. Forman, D. Lessley, A. Lau, and C. Garson, “Development and assessment of a device and method for studying the mechanical interactions between shoes and playing surfaces in situ at loads and

rates generated by elite athletes," *Sport. Biomech.*, vol. 11, no. 3, pp. 414–429, 2012, doi: 10.1080/14763141.2011.650188.

[8] J. Ekstrand, M. Hägglund, K. Kristenson, H. Magnusson, and M. Waldén, "Fewer ligament injuries but no preventive effect on muscle injuries and severe injuries: An 11-year follow-up of the UEFA Champions League injury study," *Br. J. Sports Med.*, 2013, doi: 10.1136/bjsports-2013-092394.

[9] A. Karamanoukian, J. P. Boucher, R. Labbé, and N. Vignais, "Validation of Instrumented Football Shoes to Measure On-Field Ground Reaction Forces," *Sensors*, vol. 22, no. 10, 2022, doi: 10.3390/s22103673.

[10] R. L. Hansen, "LOWER EXTREMITY INJURY INCIDENCE AND ATHLETIC," no. May, 2019.

[11] A. Castillo-Domínguez *et al.*, "The Influence of Stud Characteristics of Football Boots Regarding Player Injuries," *Int. J. Environ. Res. Public Health*, vol. 20, no. 1, 2023, doi: 10.3390/ijerph20010720.

[12] D. McGhie and G. Ettema, "Biomechanical analysis of traction at the shoe-surface interface on third-generation artificial turf," *Sport. Eng.*, vol. 16, no. 2, pp. 71–80, Jun. 2013, doi: 10.1007/s12283-013-0115-1.

[13] J. Sánchez-Sánchez, P. Haxaire, J. García Unanue, J. L. Felipe, A. M. Gallardo, and L. Gallardo, "Determination of mechanical properties of artificial turf football pitches according to structural components," *Proc. Inst. Mech. Eng. Part P J. Sport. Eng. Technol.*, vol. 232, no. 2, pp. 131–139, 2018, doi: 10.1177/1754337117717803.

[14] A. Thomson, D. Rennie, and U. Kingdom, "Evolution of Natural Grass Playing Surfaces," pp. 322–327, 2016.

[15] J. Sánchez-Sánchez, J. L. Felipe, P. Burillo, J. Del Corral, and L. Gallardo,

"Effect of the structural components of support on the loss of mechanical properties of football fields of artificial turf," *Proc. Inst. Mech. Eng. Part P J. Sport. Eng. Technol.*, vol. 228, no. 3, pp. 155–164, 2014, doi: 10.1177/1754337114527276.

[16] N. M. Schrier, J. W. Wannop, R. T. Lewinson, J. Worobets, and D. Stefanyshyn, "Shoe traction and surface compliance affect performance of soccer-related movements," *Footwear Sci.*, vol. 6, no. 2, pp. 69–80, 2014, doi: 10.1080/19424280.2014.886302.

[17] J. W. Wannop and D. J. Stefanyshyn, "The effect of normal load, speed and moisture on footwear traction," *Footwear Sci.*, vol. 4, no. 1, pp. 37–43, 2012, doi: 10.1080/19424280.2011.653992.

[18] A. Thomson, R. Whiteley, M. Wilson, and C. Bleakley, "Correction: Six different football shoes, one playing surface and the weather; Assessing variation in shoe-surface traction over one season of elite football (PLoS ONE (2019) 14: 4 (e0216364) DOI: 10.1371/journal.pone.0216364)," *PLoS One*, vol. 14, no. 6, pp. 1–13, 2019, doi: 10.1371/journal.pone.0218865.

[19] K. B. Arbogast, J. Sorochan, A. Mcnitt, and T. Serensits, "on synthetic turf," pp. 1–26.

[20] C. Webb, S. Forrester, and P. Fleming, "Rotational traction behaviour of artificial turf," *Procedia Eng.*, vol. 72, no. 0, pp. 853–858, 2014, doi: 10.1016/j.proeng.2014.06.144.

[21] P. P. Ganason and T. P. Ganason, "Shoe surface traction and impact tester," *Footwear Sci.*, vol. 7, pp. S155–S157, Jun. 2015, doi: 10.1080/19424280.2015.1039083.

[22] Z. B. Barrons, M. J. S. Esposito, D. J. Stefanyshyn, and J. W. Wannop, "The

traction requirements of female and male basketball players," *Footwear Sci.*, vol. 0, no. 0, pp. 1–7, 2022, doi: 10.1080/19424280.2022.2141899.

[23] B. Keshvari, J. Mitternacht, V. Senner, and R. Article, "Measuring variation in vertical ground reaction force for football boot midsoles, playing surfaces and football speciic movements," pp. 1–19, 2022, [Online]. Available: https://doi.org/10.21203/rs.3.rs-1614221/v1.

[24] N. Smith, R. Dyson, and L. Janaway, "Ground reaction force measures when running in soccer boots and soccer training shoes on a natural turf surface," *Sport. Eng.*, 2004, doi: 10.1007/bf02844054.

[25] S. I. Ismail, H. Nunome, F. G. Lysdal, U. G. Kersting, and Y. Tamura, "Futsal playing surface characteristics significantly affect perceived traction and change of direction performance among experienced futsal players," *Sport. Biomech.*, vol. 00, no. 00, pp. 1–12, 2022, doi: 10.1080/14763141.2022.2143415.

[26] R. Kent, J. L. Forman, J. Crandall, and D. Lessley, "The mechanical interactions between an American football cleat and playing surfaces in-situ at loads and rates generated by elite athletes: a comparison of playing surfaces," *Sport. Biomech.*, vol. 14, no. 1, pp. 1–17, 2015, doi: 10.1080/14763141.2015.1024277.

[27] Haldex, "Traction Systems - Haldex," 2008, [Online]. Available: http://www.haldex.com/sv/GLOBAL/Om-Haldex/The-Haldex-business/Traction-Systems/.

[28] S. Kuhlman, M. Sabick, R. Pfeiffer, B. Cooper, and J. Forhan, "Effect of loading condition on the traction coefficient between shoes and artificial turf surfaces," *Proc. Inst. Mech. Eng. Part P J. Sport. Eng. Technol.*, vol. 224, no. 2, pp. 155–165, 2010, doi: 10.1243/17543371JSET56.

[29] T. J. Serensits and A. S. McNitt, "Comparison of Rotational Traction of Athletic

Footwear on Varying Playing Surfaces Using Different Normal Loads," *Appl. Turfgrass Sci.*, vol. 11, no. 1, p. ATS-2013-0073-RS, 2014, doi: 10.2134/ats-2013-0073-rs.

[30] A. Thomson, R. Whiteley, and C. Bleakley, "Higher shoe-surface interaction is associated with doubling of lower extremity injury risk in football codes: A systematic review and meta-analysis," *Br. J. Sports Med.*, vol. 49, no. 19, pp. 1245–1252, 2015, doi: 10.1136/bjsports-2014-094478.

[31] G. J. Chatterton, "Assessing lower limb muscle parameters in high-speed running on different surfaces using inertial motion capture," pp. 1–6, 2022.

[32] J. Kang, S. Ryu, H. Gil, and S. Park, "applied sciences Effects of Modified Outsole Patterns in Tennis Shoes on Frictional Force and Biomechanical Variables of Lower Extremity Joints," 2023.

[33] J. W. Wannop *et al.*, "The mechanical interactions between an American football cleat and playing surfaces in-situ at loads and rates generated by elite athletes: a comparison of playing surfaces," *Footwear Sci.*, vol. 11, no. 3, pp. 161–167, 2019, doi: 10.1080/19424280903410062.

[34] "12_24V DC Worm Drive Geared Motor 600W Assorted ratios." .

[35] "Slip-Ring Square-Drive Rotary Torque Sensor with Encoder TRD305 _ FSH01976." .

[36] "SyRen 50A Regenerative Motor Driver." [Online]. Available: http://www.superdroidrobots.com/shop/item.aspx/syren-50a-regenerative-motor-driver/1197/.

[37] A. Thomson, C. Bleakley, W. Holmes, E. Hodge, D. Paul, and J. W. Wannop, "Rotational traction of soccer football shoes on a hybrid reinforced turf system and natural grass," *Footwear Sci.*, vol. 14, no. 1, pp. 58–69, 2022, doi:

10.1080/19424280.2022.2038690.

[38] K. A. Severn, P. R. Fleming, J. D. Clarke, and M. J. Carre, “Science of synthetic turf surfaces: Investigating traction behaviour,” *Proc. Inst. Mech. Eng. Part P J. Sport. Eng. Technol.*, vol. 225, no. 3, pp. 147–158, 2011, doi: 10.1177/1754337111408980.

[39] K. Kinnunen *et al.*, “Coupling with adjustable torsional stiffness,” *Proc. Est. Acad. Sci.*, vol. 70, no. 4, pp. 470–476, 2021, doi: 10.3176/proc.2021.4.14.

[40] X. B. Nguyen, T. Komatsuzaki, and H. T. Truong, “Adaptive parameter identification of Bouc-wen hysteresis model for a vibration system using magnetorheological elastomer,” *Int. J. Mech. Sci.*, vol. 213, no. October 2021, p. 106848, 2022, doi: 10.1016/j.ijmecsci.2021.106848.

[41] P. Skrzypacz, D. Nurakhmetov, and D. Wei, “Generalized stiffness and effective mass coefficients for power-law Euler–Bernoulli beams,” *Acta Mech. Sin. Xuebao*, 2020, doi: 10.1007/s10409-019-00912-8.

[42] H. Cheng, Y. Wang, Y. Tang, X. Zhao, H. Wang, and J. Zhai, “COLLABORATIVE ADAPTIVE CONTROL STRATEGY FOR ROTOR INERTIA AND DAMPING COEFFICIENT OF VIRTUAL SYNCHRONOUS GENERATOR,” *UPB Sci. Bull. Ser. C Electr. Eng. Comput. Sci.*, 2022.

Appendix A: Research Work Outcomes

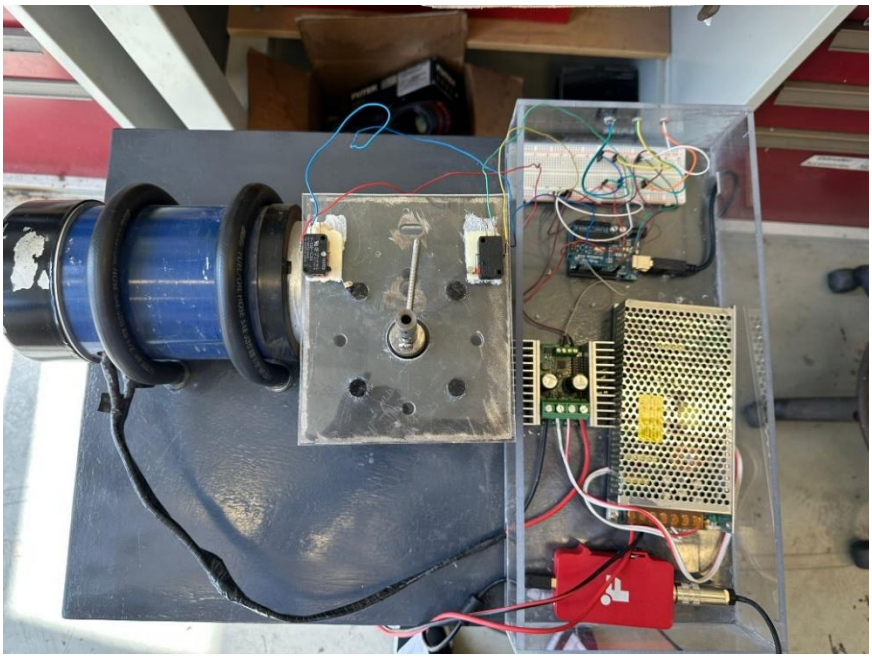

Figure 1A: Top view of developed add-on system

Figure 2A: Testing of built automated traction machine of the field

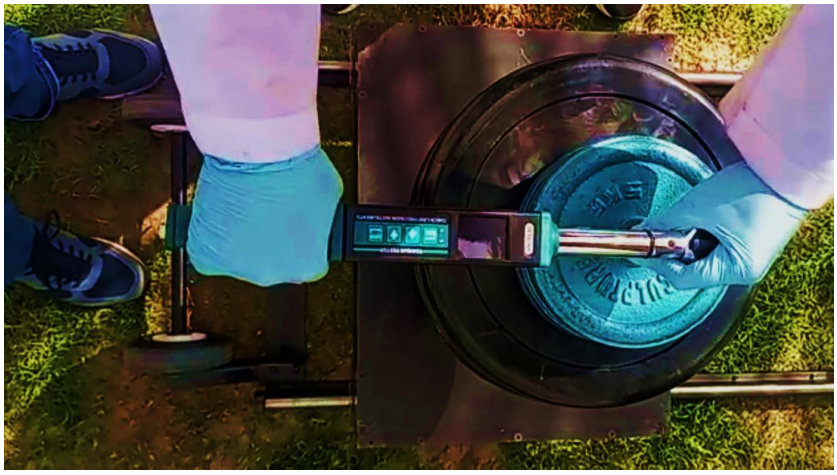

Figure 3A. Testing of manually operated traction machine

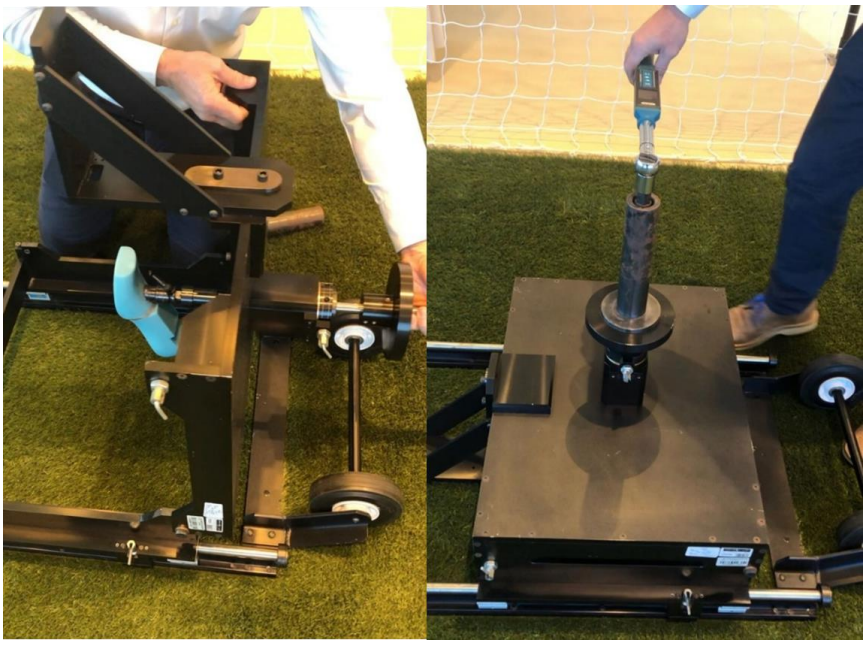

Figure 4A. Demonstration for the testing shoe attachment position and working process of torque wrench.

Arduino program

```
#include <SyRenSimplified.h>

SyRenSimplified SR;

int ls1=4,ls2=5;

int pwrbtn=6,cwbtn=7,ccwbtn=8;

int pwr,cw,ccw,LS1,LS2;
```

```
void setup()
{
  SyRenTXPinSerial.begin(9600); // This is the baud rate you chose with the DIP switches.
pinMode(ls1,INPUT_PULLUP);
pinMode(ls2,INPUT_PULLUP);
pinMode(cwbtn,INPUT_PULLUP);
pinMode(ccwbtn,INPUT_PULLUP);
pinMode(pwrbtn,INPUT_PULLUP);
}
void loop()
{
  cw=digitalRead(cwbtn);
  ccw=digitalRead(ccwbtn);
  pwr=digitalRead(pwrbtn);
  LS1=digitalRead(ls1);
  LS2=digitalRead(ls2);
if (cw == LOW && LS1 == HIGH){
  SR.motor(127);  // Go forward at full power.
  }
if(LS1 == LOW){
  SR.motor(0);    // Stop.
  }
if (ccw == LOW && LS2 == HIGH){
  SR.motor(-127);  // Go Reverse at full power.
```

```
  }
if(LS2 == LOW){
  SR.motor(0);    // Stop.
  }
if(pwr == LOW){
  SR.motor(0);    // Stop.
}
}
```

Appendix B : Data Plots

Real-time data plots for the individual experiments

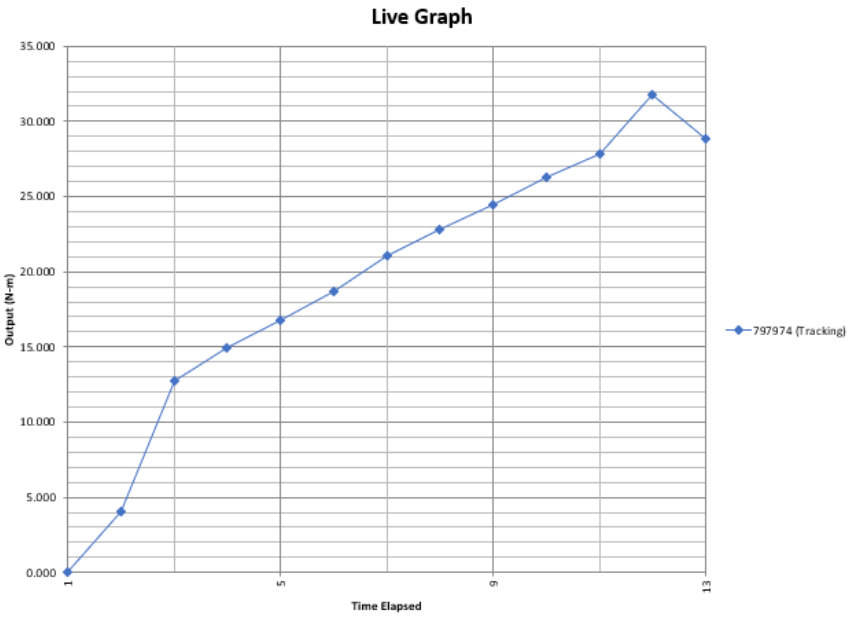

Figure 1B: Torque vs angle plot of 588 N at 25 rpm for natural grass

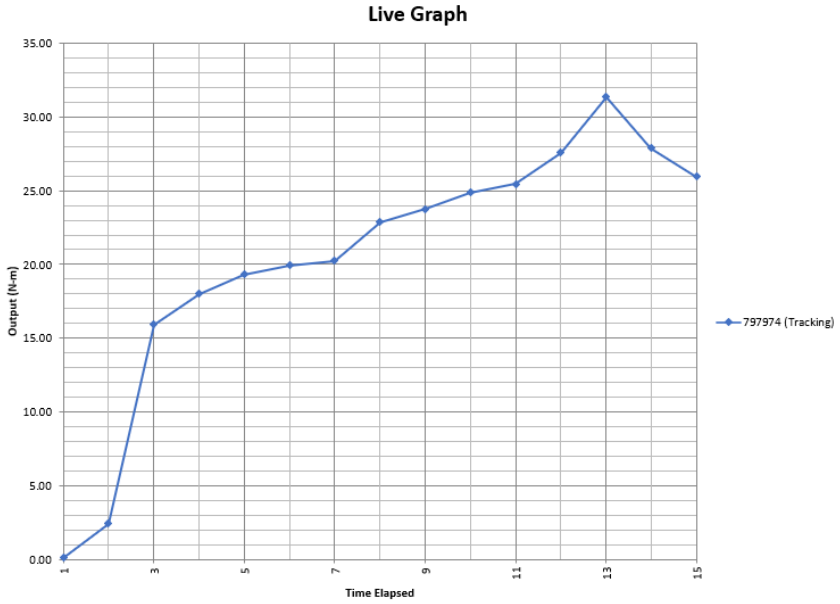

Figure 2B: Torque vs angle plot of 588 N at 30 rpm for artificial grass

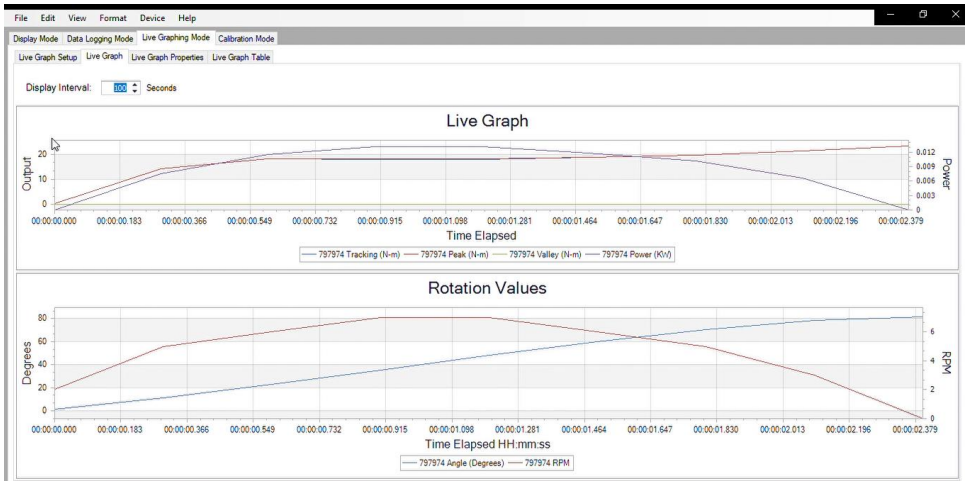

Figure 3B: Real-time data plot in Futek rotary sensor application

Appendix C : Poster Presentation

Design and development of a safe shoe design facility for decreasing lower injuries in football

Mohammad Farhan[1], Mohammad Roshun Paurobally[1], Athol Thomson[2]
[1]Department of Mechanical and Industrial Engineering, College of Engineering, Qatar University, 2713, Doha, Qatar
[2]Aspetar Orthopaedic and Sports Medicine Hospital, Doha, Qatar

Abstract

Lower limb injuries in sports like football are a very common issue due to insufficient traction during sudden maneuvers between the shoes and playing surfaces. The main goal of this project is to design and build a smart mechatronic-based add-on system for the traction machine used by Aspetar, to have automated measurement of torsional stiffness characteristics of shoe/grass interactions. This equipment is used to measure the mechanical interactions between an athlete's shoes and the grass of the playing surface. All the mechanical interactions between the shoes and the surface are currently measured by a manually operated torque wrench. This mechatronic add-on enhances the capability and accuracy of the manual version and provides real-time data for post-processing. In addition, it will improve repeatability and provide reliable results for comparison purposes. The output of this research will help to choose the best football surface and shoe combination.

Manual Traction Testing Machine

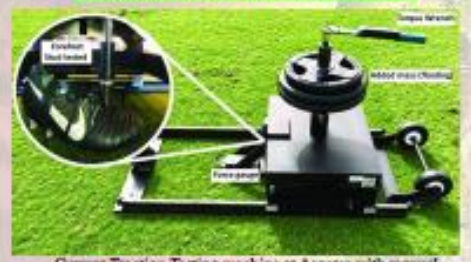

Current Traction Testing machine at Aspetar with manual operation

System components

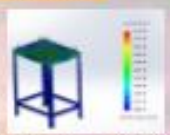

Design of Add-on Frame to hold the motor and the other components

DC Geared Motor

FUTEK TRD305 sensor

Electronics interface and microcontroller

Five common injuries in football

Causes of Injury

1. Sudden powerful movements, such as sprinting, lunging
2. Roll or twist of ankle inwards
3. Sudden movements such as kicking
4. Sudden twisting motion or a side impact

Complete System with Add-on

Complete system with add-on, motor, and sensor

Sensor Output

Variation of instantaneous and peak torques output (top plot) and angle and motor angular speed with time (bottom plot)

Torque/Angle curve

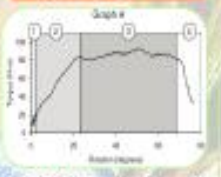

Typical Torque/Angle curve for football shoes

Conclusions

1. A mechatronic-based add-on has been developed to automate the measurement of torque and angle in football shoe-surface traction.
2. This improves the accuracy of measurements, provides data in real-time, and allows many tests to be carried out in a short time.
3. The variation of the torque with angle over time is displayed and can be used to compare different shoe/surface interactions.
4. The torsional stiffness can be obtained at any instant as well as the rate of change of the stiffness.
5. The output from this research shows a better understanding of optimal shoe/surface conditions to prevent injuries.

Effect Of Incorporating Nanosized Hafnium Carbide In Ni-P Matrix Synthesized Through Electroless Method

Mohammad Farhan[1,2], Osama Fayyaz[1], R. A. Shakoor[1*]
[1]Center for Advanced Materials (CAM), Qatar University, 2713, Doha, Qatar
[2]Department of Mechanical and Industrial Engineering, College of Engineering, Qatar University, 2713, Doha, Qatar

Abstract

- Mitigating corrosion by enhancing the surface properties of component is one of the most vital areas of research.
- Nickel-based metallic coatings are well known for their adequate performance against corrosion and are studied to improve their mechanical properties.
- In this study, novel nanosized hafnium carbide species were utilized as reinforcement in the Ni-P matrix synthesized through electroless deposition on carbon steel.
- Effect of increasing concentration of nanosized hafnium carbide species is explored in terms of structural, compositional, morphological, topographical, mechanical, and electrochemical properties.
- The attractive properties of nanosized hafnium carbide reinforced nanocomposite coating provide a tempting option for their application in various industries such as aerospace, automobile, electronic, and oil & gas industry.

Methodology and Deposition Schematics

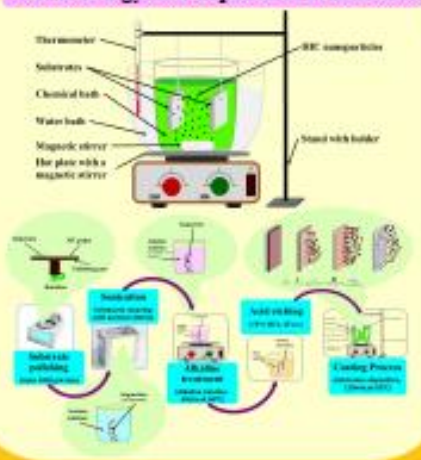

Morphology Results

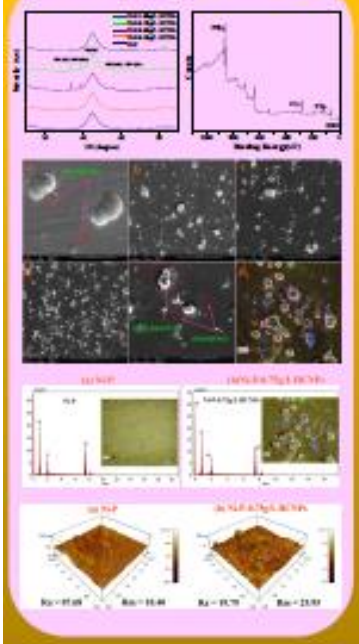

Corrosion Performance

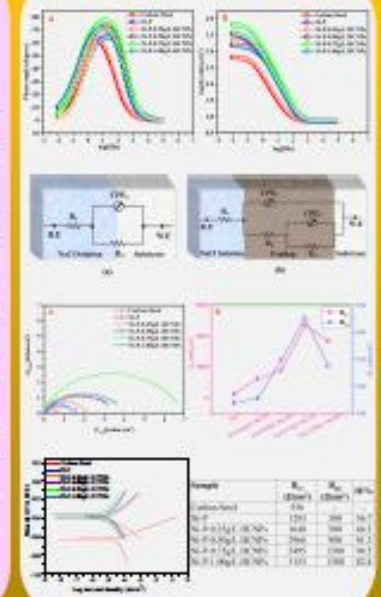

Mechanical Properties

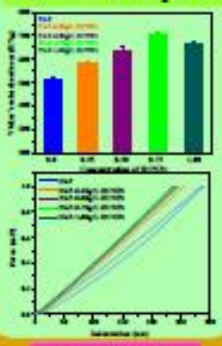

Conclusion

- Hafnium carbide reinforced nanocomposite coatings with varying contents of HfC were successfully developed through an electroless deposition process.
- Most promising results were obtained for 0.75g/L concentration with a surface hardness of 700 HV_{50} on the Vickers scale showing an enhancement of around 40%.
- Electrochemical measurement indicates an improvement of almost 95% in corrosion resistance.

Acknowledgment: The present work is supported by Qatar University Grants IRCC-2022-491. Corresponding Author - shakoor@qu.edu.qa

Appendix D: Posters Publication

Mohammad Farhan, Mohammad Roshun Paurobally, Athol Thomson, "Design and Development of a Safe Shoe Design Facility for Decreasing Lower Injuries in Football", **QUARFE 2022, 3-4 October 2022**

Mohammad Farhan, Osama Fayyaz, R.A. Shakoor, "Effect Of Incorporating Nanosized Hafnium Carbide In Ni-P Matrix Synthesized Through Electroless Method", **QUARFE 2022, 3-4 October 2022**